

---

# A GENERALIZED FRAMEWORK FOR MULTISCALE STATE-SPACE MODELING WITH NESTED NONLINEAR DYNAMICS: AN APPLICATION TO BAYESIAN LEARNING UNDER SWITCHING REGIMES

---

**Nayely Vélez-Cruz**  
School of Complex Adaptive Systems  
Arizona State University  
Tempe, AZ 85282  
nvelezcr@asu.edu

**Manfred D. Laubichler**  
School of Complex Adaptive Systems  
Arizona State University  
Tempe, AZ 85282  
Manfred.Laubichler@asu.edu

October 31, 2024

## ABSTRACT

In this work, we introduce a generalized framework for multiscale state-space models that incorporates nested nonlinear dynamics, with a specific focus on Bayesian learning under switching regimes. Our framework captures the complex interactions between fast and slow processes within systems, allowing for the analysis of how these dynamics influence each other across various temporal scales. We model these interactions through a hierarchical structure in which finer time-scale dynamics are nested within coarser ones, facilitating feedback between the scales. To promote the practical application of our framework, we address the problem of identifying switching regimes and transient dynamics. In particular, we develop a Bayesian learning approach to estimate latent states and indicators corresponding to switching dynamics, enabling the model to adapt effectively to regime changes. We employ Sequential Monte Carlo, or particle filtering, for inference. We illustrate the utility of our framework through simulations. The results demonstrate that our Bayesian learning approach effectively tracks state transitions and achieves accurate identification of switching dynamics in multiscale systems.

## 1 Introduction

In complex systems, processes operate across multiple time scales, such as rapid fluctuations in environmental conditions, intermediate responses like population dynamics, and slower shifts such as ecosystem succession or climate change. These dynamics are often nested, with fast processes embedded within slower ones. Fine-scale, rapid changes can accumulate over time to influence large-scale trends, while slower processes provide the conditions for fast dynamics to unfold.

This interplay between processes at different time scales can lead to transient behaviors, where a system remains in one dynamic state for an extended period before abruptly shifting to another [4]. In ecological systems, these dynamics often manifest as long transients—periods of apparent stability followed by sudden regime shifts. These shifts can occur without any obvious external trigger, driven instead by internal processes or responses to environmental variability [6]. During these phases, a system may exhibit consistent behavior over time before transitioning to a different dynamic regime, which could involve altered oscillatory patterns or a completely new structure. Such transitions are difficult to predict, as they are nonlinear, involve systems operating at multiple interacting scales, and are influenced by stochasticity [5, 2].

Understanding these multiscale and nonlinear interactions is essential for anticipating regime shifts, which are often most consequential at the coarsest time scales, where changes in slow-moving processes like ecosystem succession or long-term climate changes lead to impactful, irreversible transitions [6]. In contrast, finer time scales capture rapid,

fluctuations, such as daily population variations or nutrient cycles, which do not induce permanent changes unless their effects accumulate over time.

Recognizing the critical roles these dynamics play informs our approach to modeling them effectively. In this work, we propose a generalized multiscale state-space modeling framework with nested nonlinear dynamics. This framework, which is an extension of our work in [7], is designed to incorporate interactions between any number of temporal scales, enabling a comprehensive representation of complex systems where localized, rapid changes can propagate and influence slower, broader-scale phenomena and vice versa. In addition to modeling interactions across time scales, we also account for switching dynamics within the broadest time scale. In particular, we introduce a Bayesian learning approach to estimate the latent states and identify the underlying dynamic regimes, allowing for flexible modeling of systems where the dynamics may switch between different models over time.

## 2 Model Description

At each time scale  $l$ , the latent state  $\mathbf{x}_{d,t_l}^{[l]}$  for individual  $d$  evolves based on its previous state  $\mathbf{x}_{d,t_{l-1}}^{[l]}$ , the entire trajectory of the finer time scales  $\left\{ \mathbf{x}_{d,1:T_{l'}}^{[l']} \right\}_{l'=1}^{l-1}$ , and the states from the coarser time scales  $\left\{ \mathbf{x}_{d,t_{l'-1}}^{[l']} \right\}_{l'=l+1}^L$ . The dependence on the coarser time scale states  $\mathbf{x}_{d,t_{l'-1}}^{[l']}$  reflects the influence of slower, large-scale processes, which can shape the overall context in which finer-scale dynamics unfold, providing broader temporal trends or constraints from longer time horizons. This structure allows feedback across time scales, enabling interactions between processes operating at different temporal resolutions. Additionally, the model includes additive process noise,  $\mathbf{w}_{d,t_{l-1}}^{[l]}$ , to account for stochastic influences. The state transition equation for time scale  $l$  and individual (or more generally, entity)  $d$ , is given by:

$$\mathbf{x}_{d,t_l}^{[l]} = f_l \left( \mathbf{x}_{d,t_{l-1}}^{[l]}, \left\{ \mathbf{x}_{d,1:T_{l'}}^{[l']} \right\}_{l'=1}^{l-1}, \left\{ \mathbf{x}_{d,t_{l'-1}}^{[l']} \right\}_{l'=l+1}^L \right) + \mathbf{w}_{d,t_{l-1}}^{[l]} \quad (1)$$

$$\mathbf{y}_{d,t_l}^{[l]} = h_l(\mathbf{x}_{d,t_l}^{[l]}) + \mathbf{v}_{d,t_l}^{[l]} \quad (2)$$

The function  $f_l$  captures the transition dynamics for the latent state at time scale  $l$ , incorporating the previous state, the entire trajectory from all finer time scales, and additive process noise  $\mathbf{w}_{d,t_{l-1}}^{[l]}$ . The measurement model equation for  $\mathbf{y}_{d,t_l}^{[l]}$  describes how the measurements at time scale  $l$  (denoted as  $\mathbf{y}_{d,t_l}^{[l]}$ ) relates to the latent state  $\mathbf{x}_{d,t_l}^{[l]}$ . The function  $h_l(\mathbf{x}_{d,t_l}^{[l]})$  maps the latent state to the measurements, while  $\mathbf{v}_{d,t_l}^{[l]}$  represents the measurement noise that accounts for measurement errors or uncertainties in the measurements.

Table 1: Notation Table

Variable	Description
$\mathbf{x}_{d,t_l}^{[l]}$	Latent state of individual $d$ at time scale $l$ and time $t_l$ .
$\left\{ \mathbf{x}_{d,1:T_{l'}}^{[l']} \right\}_{l'=1}^{l-1}$	The entire trajectory of states from all finer time scales, representing the influences across time scales.
$\left\{ \mathbf{x}_{d,t_{l'-1}}^{[l']} \right\}_{l'=l+1}^L$	The set of states from all coarser time scales at the previous coarse time point, capturing the broader, slower dynamics that influence the finer time scale processes.
$f_l(\cdot)$	Transition function for the latent state at time scale $l$ , incorporating feedback from finer and coarser time scales.
$B_{d,d'}^{[l]}$	Interaction matrix capturing the interactions between individuals $d$ and $d'$ at time scale $l$ .
$\mathbf{A}_{t_l}^{[l]}$	Adjacency matrix capturing interactions between dimensions of the state vector for individual $d$ at time $t_l$ .
$\mathbf{w}_{d,t_{l-1}}^{[l]}$	Process noise for state transition at time scale $l$ , representing random fluctuations in the system at time $t_l$ .
$\mathbf{y}_{d,t_l}^{[l]}$	Measurements at time scale $l$ , measured at time $t_l$ .
$h_l(\cdot)$	Measurement function mapping the latent state at time scale $l$ to the measurements.

$\mathbf{v}_{d,t_l}^{[l]}$	Measurement noise at time scale $l$ , accounting for measurement errors or noise in the measurements at time $t_l$ .
$t_l$	Time index corresponding to the time scale $l$ , representing different resolutions of time depending on $l$ .
$L$	The total number of time scales in the model, with the finest time scale $l = 1$ and the coarsest $l = L$ .
$l'$	An index representing all time scales from 1 to $l - 1$ , referring to finer time scales.

## 2.1 Example: $L = 2$

To illustrate the model, consider the case of  $L = 2$ , where there are two time scales. The finest time scale  $l = 1$  may represent fast processes such as development, while the coarser time scale  $l = 2$  may represent slower processes such as heredity or population dynamics. At the finest time scale  $l = 1$ , the latent state evolves as:

$$\mathbf{x}_{d,t_1}^{[1]} = f_1 \left( \mathbf{x}_{d,t_1-1}^{[1]}, \mathbf{x}_{d,t_2-1}^{[2]} \right) + \mathbf{w}_{d,t_1-1}^{[1]} \quad (3)$$

At the coarser time scale  $l = 2$ , the latent state depends on the full trajectory of the finer time scale  $l = 1$ , evolving as:

$$\mathbf{x}_{d,t_2}^{[2]} = f_2 \left( \mathbf{x}_{d,t_2-1}^{[2]}, \mathbf{x}_{d,1:T_1}^{[1]} \right) + \mathbf{w}_{d,t_2-1}^{[2]} \quad (4)$$

The measurement at each time scale follows:

$$\mathbf{y}_{d,t_1}^{[1]} = h_1 \left( \mathbf{x}_{d,t_1}^{[1]} \right) + \mathbf{v}_{d,t_1}^{[1]} \quad (5)$$

$$\mathbf{y}_{d,t_2}^{[2]} = h_2 \left( \mathbf{x}_{d,t_2}^{[2]} \right) + \mathbf{v}_{d,t_2}^{[2]} \quad (6)$$

## 2.2 Example: $L = 3$

To illustrate the model with three time scales, consider the case of  $L = 3$ , where there are three nested temporal scales. The finest time scale  $l = 1$  may represent fast processes such as cellular signaling, the intermediate time scale  $l = 2$  may represent developmental processes, and the coarsest time scale  $l = 3$  may represent evolutionary or population-level dynamics. At the finest time scale  $l = 1$ , the latent state evolves as:

$$\mathbf{x}_{d,t_1}^{[1]} = f_1 \left( \mathbf{x}_{d,t_1-1}^{[1]}, \mathbf{x}_{d,t_2-1}^{[2]}, \mathbf{x}_{d,t_3-1}^{[3]} \right) + \mathbf{w}_{d,t_1-1}^{[1]} \quad (7)$$

At the intermediate time scale  $l = 2$ , the latent state depends on the full trajectory of the finer time scale  $l = 1$ , evolving as:

$$\mathbf{x}_{d,t_2}^{[2]} = f_2 \left( \mathbf{x}_{d,t_2-1}^{[2]}, \mathbf{x}_{d,1:T_1}^{[1]}, \mathbf{x}_{d,t_3-1}^{[3]} \right) + \mathbf{w}_{d,t_2-1}^{[2]} \quad (8)$$

At the coarsest time scale  $l = 3$ , the latent state is influenced by both finer time scales, evolving as:

$$\mathbf{x}_{d,t_3}^{[3]} = f_3 \left( \mathbf{x}_{d,t_3-1}^{[3]}, \mathbf{x}_{d,1:T_1}^{[1]}, \mathbf{x}_{d,1:T_2}^{[2]} \right) + \mathbf{w}_{d,t_3-1}^{[3]} \quad (9)$$

The measurements at each time scale are modeled as:

$$\mathbf{y}_{d,t_1}^{[1]} = h_1 \left( \mathbf{x}_{d,t_1}^{[1]} \right) + \mathbf{v}_{d,t_1}^{[1]} \quad (10)$$

$$\mathbf{y}_{d,t_2}^{[2]} = h_2 \left( \mathbf{x}_{d,t_2}^{[2]} \right) + \mathbf{v}_{d,t_2}^{[2]} \quad (11)$$

$$\mathbf{y}_{d,t_3}^{[3]} = h_3 \left( \mathbf{x}_{d,t_3}^{[3]} \right) + \mathbf{v}_{d,t_3}^{[3]} \quad (12)$$

## 2.3 Introducing Interaction Matrices $A$ and $B$

To capture the dependencies between different dimensions of the state vector within the same individual at time  $t_l$ , we introduce an adjacency matrix  $\mathbf{A}_{t_l}^{[l]}$ . This matrix effectively models the interactions among the elements of the state vector  $\mathbf{x}_{d,t_l}^{[l]}$ , allowing us to account for how each state component influences others at a given time. For instance, in a

biological system, the state components might represent different gene expression levels, where the adjacency matrix reflects regulatory relationships among genes. For finer time scales  $l < L$ , the state transition model is given by:

$$\mathbf{x}_{d,t_l}^{[l]} = f_l \left( \mathbf{A}_{t_l}^{[l]} \mathbf{x}_{d,t_l-1}^{[l]}, \left\{ \mathbf{x}_{d,1:T_{l'}}^{[l']} \right\}_{l'=1}^{l-1}, \left\{ \mathbf{x}_{d,t_{l'}-1}^{[l']} \right\}_{l'=l+1}^L \right) + \mathbf{w}_{d,t_l-1}^{[l]} \quad (13)$$

Next, to account for interactions between different individuals  $d$  and  $d'$  at the coarsest time scale  $L$ , we introduce an interaction matrix  $\mathbf{B}^{[L]}$ . This matrix influences the evolution of the latent states by capturing how the states of different individuals affect each other. For example, in social networks, the interaction matrix can represent the influence one individual's state may have on another. At the coarsest time scale  $l = L$ , the updated state transition model incorporates the interaction matrix  $\mathbf{B}^{[L]}$ :

$$\mathbf{x}_{d,t_L}^{[L]} = f_L \left( \mathbf{A}_{t_L}^{[L]} \mathbf{x}_{d,t_L-1}^{[L]}, \left\{ \mathbf{x}_{d,1:T_{l'}}^{[l']} \right\}_{l'=1}^{L-1}, \sum_{d' \neq d} B_{d,d'}^{[L]} \mathbf{x}_{d',t_L-1}^{[L]} \right) + \mathbf{w}_{d,t_L-1}^{[L]} \quad (14)$$

### 3 Bayesian Learning Under Switching Regimes

We propose a Bayesian approach for learning the unknown states at different time scales, while restricting the switching regime to the coarsest time scale  $L$ . Specifically, let  $s_{d,t_L}^{[L]} = m$  for  $m = 1, \dots, M$  denote the indicator corresponding to model (or regime)  $m$  for time scale  $L$  at time step  $t_L$  for individual  $d$ . The objective is to estimate the unknown states  $\mathbf{x}_{d,t_l}^{[l]}$  for  $t_l = 1, \dots, T_l$  and  $l = 1, \dots, L$ , and the unknown model indicators  $s_{d,t_L}^{[L]}$  at the coarsest time scale  $L$ . For the finer time scales  $l < L$ , the state evolves as:

$$\mathbf{x}_{d,t_l}^{[l]} = f_l \left( \mathbf{A}_{t_l}^{[l]} \mathbf{x}_{d,t_l-1}^{[l]}, \left\{ \mathbf{x}_{d,1:T_{l'}}^{[l']} \right\}_{l'=1}^{l-1}, \left\{ \mathbf{x}_{d,t_{l'}-1}^{[l']} \right\}_{l'=l+1}^L \right) + \mathbf{w}_{d,t_l-1}^{[l]} \quad (15)$$

At the coarsest time scale  $l = L$ , the state evolves according to the model corresponding to  $s_{d,t_L}^{[L]} = m$ :

$$\mathbf{x}_{d,t_L}^{[L]} = f_L \left( \mathbf{A}_{t_L}^{[L]} \mathbf{x}_{d,t_L-1}^{[L]}, \left\{ \mathbf{x}_{d,1:T_{l'}}^{[l']} \right\}_{l'=1}^{L-1}, s_{d,t_L}^{[L]} = m, \sum_{d' \neq d} B_{d,d'}^{[L]} \mathbf{x}_{d',t_L-1}^{[L]} \right) + \mathbf{w}_{d,t_L-1}^{[L]} \quad (16)$$

The measurement equation is assumed to be

$$\mathbf{y}_{d,t_l}^{[l]} = h_l(\mathbf{x}_{d,t_l}^{[l]}) + \mathbf{v}_{d,t_l}^{[l]} \quad (17)$$

Note that for  $l = 1, \dots, L$   $\mathbf{w}_{d,t_l}^{[l]} \sim \mathcal{N}(\mathbf{0}, \Sigma_{\mathbf{w}_d}^{[l]})$  and  $\mathbf{v}_{d,t_l}^{[l]} \sim \mathcal{N}(\mathbf{0}, \Sigma_{\mathbf{v}_d}^{[l]})$  are additive Gaussian noise terms. The function  $h_l$  applies a rotation matrix, transforming the state  $\mathbf{x}_{d,t_l}^{[l]}$  to the measurement space.

This model is summarized by the following hierarchy:

$$\begin{aligned} \mathbf{x}_{d,t_l}^{[l]} | \mathbf{x}_{d,t_l-1}^{[l]}, \left\{ \mathbf{x}_{d,1:T_{l'}}^{[l']} \right\}_{l'=1}^{l-1}, \left\{ \mathbf{x}_{d,t_{l'}-1}^{[l']} \right\}_{l'=l+1}^L &\sim \mathcal{N} \left( \mathbf{x}_{d,t_l}^{[l]} | \mathbf{x}_{d,t_l-1}^{[l]}, \left\{ \mathbf{x}_{d,1:T_{l'}}^{[l']} \right\}_{l'=1}^{l-1}, \left\{ \mathbf{x}_{d,t_{l'}-1}^{[l']} \right\}_{l'=l+1}^L, \Sigma_{\mathbf{w}_d}^{[l]} \right), \quad \text{for } l < L \\ \mathbf{x}_{d,t_L}^{[L]} | \mathbf{x}_{d,t_L-1}^{[L]}, \left\{ \mathbf{x}_{d,1:T_{l'}}^{[l']} \right\}_{l'=1}^{L-1}, s_{d,t_L}^{[L]} = m &\sim \mathcal{N} \left( \mathbf{x}_{d,t_L}^{[L]} | \mathbf{x}_{d,t_L-1}^{[L]}, \left\{ \mathbf{x}_{d,1:T_{l'}}^{[l']} \right\}_{l'=1}^{L-1}, s_{d,t_L}^{[L]}, \Sigma_{\mathbf{w}_d}^{[L]} \right) \\ \mathbf{y}_{d,t_l}^{[l]} | \mathbf{x}_{d,t_l}^{[l]} &\sim \mathcal{N} \left( \mathbf{y}_{d,t_l}^{[l]} | \mathbf{x}_{d,t_l}^{[l]}, \Sigma_{\mathbf{v}_d}^{[l]} \right), \quad \text{for } l = 1, \dots, L \\ s_{d,t_L}^{[L]} | \mathcal{S}_{d,t_L-1}^{[L]}, \boldsymbol{\pi}_{d,t_L}^{[L]} &\sim \text{Cat} \left( s_{d,t_L}^{[L]} | \mathcal{S}_{d,t_L-1}^{[L]}, \boldsymbol{\pi}_{d,t_L}^{[L]} \right) \\ \boldsymbol{\pi}_{d,t_L}^{[L]} | \boldsymbol{\alpha} &\sim \text{Dir} \left( \boldsymbol{\pi}_{d,t_L}^{[L]} | \boldsymbol{\alpha} \right) \end{aligned}$$

where  $\mathcal{S}_{d,t_L-1}^{[L]}$  denotes the set of indicators from  $t_L = 1, \dots, t_L - 1$ . The state transition distributions for  $\mathbf{x}_{d,t_l}^{[l]}$  and  $\mathbf{x}_{d,t_L}^{[L]}$  are modeled as multivariate normal distributions,  $\mathcal{N}$ . This choice is appropriate for capturing the continuous evolution of the states over time, allowing for Gaussian noise in the state transition process, represented by the known covariance matrices  $\Sigma_{\mathbf{w}_d}^{[l]}$  and  $\Sigma_{\mathbf{w}_d}^{[L]}$ . The measurement model  $\mathbf{y}_{d,t_l}^{[l]}$  given the state  $\mathbf{x}_{d,t_l}^{[l]}$  is also modeled using a Gaussian

distribution, reflecting the assumption that measurements are continuous and subject to Gaussian measurement noise represented by  $\Sigma_{\mathbf{v}_d^{[l]}}$ . The model indicators  $\mathbf{s}_{d,t_L}^{[L]}$  are drawn from a categorical distribution, Cat, which captures the discrete nature of model selection, allowing the model to switch between different regimes effectively. The model probabilities  $\pi_{d,t_L}^{[L]}$  are drawn from a Dirichlet distribution, Dir, which serves as a conjugate prior for the categorical distribution of the model indicators [3]. The Dirichlet distribution's conjugacy simplifies the inference process, allowing straightforward updates based on the counts of model selections while incorporating prior beliefs represented by the concentration parameters  $\alpha$ . The joint posterior we wish to sample from is given as follows:

$$p \left( \left\{ \mathbf{x}_{d,t_i}^{[l]}, s_{d,t_L}^{[L]}, \pi_{d,t_L}^{[L,(m)]} \right\}_{d=1, m=1, l=1, t_i=1}^{D, M, L, T_i} \mid \left\{ \mathbf{y}_{d,t_i}^{[l]} \right\}_{d=1, l=1, t_i=1}^{D, L, T_i}, \alpha, \left\{ \Sigma_{\mathbf{w}_{d,t_i}^{[l]}}, \Sigma_{\mathbf{v}_{d,t_i}^{[l]}} \right\}_{d=1, l=1}^{D, L} \right) \quad (18)$$

$$= \prod_{d=1}^D \prod_{m=1}^M \prod_{l=1}^L \prod_{t_i=1}^{T_i} p(\mathbf{x}_{d,t_i}^{[l]}, s_{d,t_L}^{[L]}, \pi_{d,t_L}^{[L,(m)]} \mid \mathbf{y}_{d,t_i}^{[l]}, \alpha_m, \Sigma_{\mathbf{w}_{d,t_i}^{[l]}}, \Sigma_{\mathbf{v}_{d,t_i}^{[l]}}) \quad (19)$$

$$\propto \prod_{d=1}^D \prod_{l=1}^L \prod_{t_i=1}^{T_i} p(\mathbf{x}_{d,t_i}^{[l]} \mid \mathbf{x}_{d,t_i-1}^{[l]}, \left\{ \mathbf{x}_{d,1:T_{l'}}^{[l']}, \right\}_{l'=1}^{l-1}, \left\{ \mathbf{x}_{d,t_{l'}-1}^{[l']}, \right\}_{l'=l+1}^L, \Sigma_{\mathbf{w}_{d,t_i}^{[l]}}) p(\mathbf{y}_{d,t_i}^{[l]} \mid \mathbf{x}_{d,t_i}^{[l]}, \Sigma_{\mathbf{v}_d^{[l]}}) \\ p(\mathbf{x}_{d,t_L}^{[L]} \mid \mathbf{x}_{d,t_L-1}^{[L]}, \left\{ \mathbf{x}_{d,1:T_{l'}}^{[l']}, \right\}_{l'=1}^{L-1}, s_{d,t_L}^{[L]}, \Sigma_{\mathbf{w}_{d,t_L}^{[L]}}) p(s_{d,t_L}^{[L]} \mid \mathcal{S}_{d,t_L-1}^{[L]}, \pi_{d,t_L}^{[L,(m)]}) p(\pi_{d,t_L}^{[L]} \mid \alpha) \quad (20)$$

With this hierarchical structure established, we can now proceed to describe the inference process, which leverages sequential Monte Carlo (SMC) to estimate the posterior distributions of the latent states and model indicators.

### 3.1 Inference via Multiscale Sequential Monte Carlo (SMC)

For inference, we leverage a multiscale Sequential Monte Carlo (SMC) approach to account for the nested structure of the dynamics. This allows us to propagate particles across different scales, handling both coarse and fine-scale dynamics simultaneously. The key novelty lies in the ability of the SMC algorithm to handle nested nonlinear dynamics at each level of the model, where the states at finer time scales feed into the coarser scales and vice versa. To simplify the weight calculation, the algorithm uses the joint prior as the proposal distribution [1] as

$$p(\mathbf{x}_{d,t_i}^{[l]}, \mathbf{x}_{d,t_i-1}^{[l]}, \left\{ \mathbf{x}_{d,1:T_{l'}}^{[l']}, \right\}_{l'=1}^{l-1}, \left\{ \mathbf{x}_{d,t_{l'}-1}^{[l']}, \right\}_{l'=l+1}^L, s_{d,t_L}^{[L]} = m, \mathcal{S}_{d,t_L-1}^{[L]}, \pi_{d,t_L}^{[L,(m)]}, \alpha_m) \quad (21)$$

$$\propto p(\mathbf{x}_{d,t_i}^{[L]} \mid \mathbf{x}_{d,t_L-1}^{[L]}, \left\{ \mathbf{x}_{d,1:T_{l'}}^{[l']}, \right\}_{l'=1}^{L-1}, s_{d,t_L}^{[L]} = m, \Sigma_{\mathbf{w}_{d,t_L}^{[L]}}) \quad (22)$$

$$p(\mathbf{x}_{d,t_i}^{[l]} \mid \mathbf{x}_{d,t_i-1}^{[l]}, \left\{ \mathbf{x}_{d,1:T_{l'}}^{[l']}, \right\}_{l'=1}^{l-1}, \left\{ \mathbf{x}_{d,t_{l'}-1}^{[l']}, \right\}_{l'=l+1}^L, \Sigma_{\mathbf{w}_{d,t_i}^{[l]}}) \quad (23)$$

$$p(s_{d,t_L}^{[L]} \mid \mathcal{S}_{d,t_L-1}^{[L]}, \pi_{d,t_L}^{[L,(m)]}) p(\pi_{d,t_L}^{[L]} \mid \alpha) \quad (24)$$

For each  $l = 1, \dots, L-1$ , where each finer scale  $l$  is nested within the coarser time scale  $l+1$ , and for each particle  $i = 1, \dots, N_s$  the states  $\mathbf{x}_{d,t_i}^{[l],(i)}$  are sampled from  $p(\mathbf{x}_{d,t_i}^{[l],(i)} \mid \mathbf{x}_{d,t_i-1}^{[l],(i)}, \left\{ \mathbf{x}_{d,1:T_{l'}}^{[l']}, \right\}_{l'=1}^{l-1}, \left\{ \mathbf{x}_{d,t_{l'}-1}^{[l']}, \right\}_{l'=l+1}^L, \Sigma_{\mathbf{w}_{d,t_i}^{[l]}})$  for  $t_i = 1, \dots, T_l$  using the standard SMC algorithm. The resampled particles from each time step  $t_i$  at time scale  $l$  serve as input to the particle filter at the coarser time scale  $l+1$  for time step  $t_i+1$ . Similarly, the output of the coarser time scale  $l+1$  particle filter at time  $t_{i+1}$  becomes an input into the finer time scale PF at the next iteration  $t_{i-1}+1$ . Then, for the coarsest time scale  $L$  the probabilities  $\pi_{d,t_L}^{[L,(m),i]}$  for selecting each model  $m = 1, \dots, M$  are sampled from the following Dirichlet distribution:

$$\pi_{d,t_L}^{[L],(i)} \mid \mathbf{s}_{d,1:t_L-1}^{[L],(i)}, \alpha \sim \text{Dir}(\alpha_1 + c_{1:t_L-1}^{[L],(1),i}, \dots, \alpha_m + c_{1:t_L-1}^{[L],(M),i}) \quad (25)$$

where  $c_{1:t_L-1}^{[L],(M),i}$  is the number of times model  $m$  has been selected up to time  $t_L-1$  and  $\alpha_m$  is the Dirichlet distribution concentration parameter for model  $m$ . Next, the model indicator  $s_{d,t_L}^{[L],(i)}$  is sampled from

$$p(s_{d,t_L}^{[L],(i)} = m \mid \mathcal{S}_{d,t_L-1}^{[L],(i)}, \mathbf{x}_{d,t_L}^{[L],(i)}, \left\{ \mathbf{x}_{d,1:T_{l'}}^{[l']}, \right\}_{l'=1}^{l-1}, \pi_{d,t_L}^{[L],(m),i}, \mathbf{y}_{d,t_L}^{[L]}) \\ \propto p(s_{d,t_L}^{[L],(i)} = m \mid \mathcal{S}_{d,t_L-1}^{[L],(i)}, \pi_{d,t_L}^{[L],(m),i}) p(\mathbf{x}_{d,t_L}^{[L],(i)} \mid \mathbf{x}_{d,t_L-1}^{[L],(i)}, \left\{ \mathbf{x}_{d,1:T_{l'}}^{[l']}, \right\}_{l'=1}^{l-1}, s_{d,t_L}^{[L],(i)} = m, \Sigma_{\mathbf{w}_{d,t_L}^{[L]}}) \\ p(\mathbf{y}_{d,t_L}^{[L],(i)} \mid \mathbf{x}_{d,t_L}^{[L],(i)}, \Sigma_{\mathbf{v}_d^{[L]}}) \quad (26)$$

It is selected by first computing the prior probability  $p(s_{d,t_L}^{[L],(i)} = m | \mathcal{S}_{d,t_L-1}^{[L],(i)}, \pi_{d,t_L}^{[L],(m),(i)})$ , which reflects how frequently the model  $m$  has been chosen in the past, weighted by the Dirichlet-distributed parameters  $\pi_{d,t_L}^{[L],(m),(i)}$ . This prior is then combined with the transition density and measurement likelihood to form a posterior distribution. From this posterior, the model indicator  $s_{d,t_L}^{[L],(i)}$  is sampled, determining the most probable model  $m$  for the current time step based on past selections and the current state and measurement dynamics. More specifically, for each model  $m$ , a new state  $\mathbf{x}_{d,t_L}^{L,(i)*}$  is sampled from

$$\mathbf{x}_{d,t_L}^{L,(i)*} = f_L \left( \mathbf{A}_{t_L}^{[L]} \mathbf{x}_{d,t_L-1}^{[L],(i)}, \left\{ \mathbf{x}_{d,1:T_{l'}}^{[l'],(i)} \right\}_{l'=1}^{L-1}, s_{d,t_L}^{[L],(i)} = m, \sum_{d' \neq d} B_{d,d'}^{[L]} \mathbf{x}_{d',t_L-1}^{[L],(i)} \right) + \mathbf{w}_{d,t_L-1}^{[L]} \quad (27)$$

and the corresponding transition densities are computed for each model

$$p(\mathbf{x}_{d,t_L}^{[L],(i)*} | \mathbf{x}_{d,t_L-1}^{[L],(i)}, \left\{ \mathbf{x}_{d,1:T_{l'}}^{[l'],(i)} \right\}_{l'=1}^{L-1}, s_{d,t_L}^{[L],(i)} = m, \Sigma_{\mathbf{w}_{d,t_L}^{[L]}}).$$

Then the likelihoods for each model are computed via

$$p(\mathbf{y}_{d,t_L}^{[l],(i)} | \mathbf{x}_{d,t_L}^{L,(i)*}, \Sigma_{\mathbf{v}_d^{[l]}}).$$

Given the selected model indicator,  $s_{d,t_L}^{[L],(i)} = m$ , a new state  $\mathbf{x}_{d,t_L}^{L,(i)}$  is again sampled from Equation 27. The particle weights are computed and then the states and indicators are resampled. These steps are summarized in Algorithm 1.

**Algorithm 1** Multiscale Particle Filter

- 
- 1: **Input:** Number of particles  $N_s$ , time scales  $L$ , measurements  $\mathbf{y}_{d,t_l}$ , transition functions  $f_l$ , Dirichlet concentration parameters  $\alpha_m$ , interaction matrices  $\mathbf{A}, \mathbf{B}$ , noise covariance matrices  $\Sigma_{\mathbf{w}}, \Sigma_{\mathbf{v}}$
  - 2: **Initialize:**
  - 3: **for** each individual  $d$  **do**
  - 4:     **for** each time scale  $l = 1, \dots, L$  **do**
  - 5:         Initialize particles  $\mathbf{x}_{d,0}^{[l],(i)}$  for  $i = 1, \dots, N_s$
  - 6:         Set initial weights  $w_{d,0}^{[l],(i)} = \frac{1}{N_s}$  for all particles
  - 7:     **end for**
  - 8: **end for**
  - 9:
  - 10: **for** each individual  $d$  **do**
  - 11:     **for** each time scale  $l = 1, \dots, L - 1$  **do**
  - 12:         **for** each time step  $t_l = 1, \dots, T_l$  **do**
  - 13:             **for** each particle  $i = 1, \dots, N_s$  **do**
  - 14:                 Sample  $\mathbf{x}_{d,t_l}^{[l],(i)}$  from
 
$$\mathbf{x}_{d,t_l}^{[l],(i)*} = f_l \left( \mathbf{A}_{t_l}^{[l]} \mathbf{x}_{d,t_{l-1}}^{[l],(i)}, \left\{ \mathbf{x}_{d,1:T_{l'}}^{[l'],(i)} \right\}_{l'=1}^{l-1}, \left\{ \mathbf{x}_{d,t_{l'}-1}^{[l'],(i)} \right\}_{l'=l+1}^L \right) + \mathbf{w}_{d,t_{l-1}}^{[l]}$$
  - 15:                 Update particle weights using the previous weights and the computed likelihood:
 
$$w_{d,t_l}^{[l],(i)} \propto w_{d,t_{l-1}}^{[l],(i)} \cdot p(\mathbf{y}_{d,t_l}^{[l]} | \mathbf{x}_{d,t_l}^{[l],(i)}, \Sigma_{\mathbf{v}_d}^{[l]})$$
  - 16:             **end for**
  - 17:             Resample particles at time step  $t_l$ , where the resampled particles serve as input to the coarser time scale  $l + 1$  at the next iteration.
  - 18:     **end for**
  - 19: **end for**
  - 20: **for** each time step  $t_L = 1, \dots, T_L$  at the coarsest time scale  $L$  **do**
  - 21:     **for** each particle  $i = 1, \dots, N_s$  **do**
  - 22:         Sample model probabilities  $\pi_{d,t_L}^{[L],(i)} \sim \text{Dir}(\alpha_1 + c_{1:t_L-1}^{[L],(1),(i)}, \dots, \alpha_M + c_{1:t_L-1}^{[L],(M),(i)})$
  - 23:         Sample model indicator  $s_{d,t_L}^{[L],(i)}$  from
 
$$p(s_{d,t_L}^{[L],(i)} = m | \mathcal{S}_{d,t_L-1}^{[L],(i)}, \mathbf{x}_{d,t_L}^{[L],(i)}, \left\{ \mathbf{x}_{d,1:T_{l'}}^{[l'],(i)} \right\}_{l'=1}^{l-1}, \pi_{d,t_L}^{[L],(m),(i)}, \mathbf{y}_{d,t_L}^{[L]})$$

$$\propto p(s_{d,t_L}^{[L],(i)} = m | \mathcal{S}_{d,t_L-1}^{[L],(i)}, \pi_{d,t_L}^{[L],(m),(i)}) p(\mathbf{x}_{d,t_L}^{[L],(i)} | \mathbf{x}_{d,t_L-1}^{[L],(i)}, \left\{ \mathbf{x}_{d,1:T_{l'}}^{[l'],(i)} \right\}_{l'=1}^{l-1}, s_{d,t_L}^{[L],(i)} = m, \Sigma_{\mathbf{w}_{d,t_L}^{[L],(i)}})$$

$$p(\mathbf{y}_{d,t_L}^{[L]} | \mathbf{x}_{d,t_L}^{[L],(i)}, \Sigma_{\mathbf{v}_d}^{[L]})$$
  - 24:         Sample new state  $\mathbf{x}_{d,t_L}^{L,(i)}$  from:
 
$$\mathbf{x}_{d,t_L}^{L,(i)} = f_L \left( \mathbf{A}_{t_L}^{[L]} \mathbf{x}_{d,t_L-1}^{[L]}, \left\{ \mathbf{x}_{d,1:T_{l'}}^{[l'],(i)} \right\}_{l'=1}^{L-1}, s_{d,t_L}^{[L],(i)} = m, \sum_{d' \neq d} \mathbf{B}_{d,d'}^{[L]} \mathbf{x}_{d',t_L-1}^{[L],(i)} \right) + \mathbf{w}_{d,t_L-1}^{[L]}$$
  - 25:         Compute the likelihood of the current observation:
  - 26:         Update particle weights using the previous weights and the computed likelihood:
 
$$w_{d,t_L}^{[L],(i)} \propto w_{d,t_L-1}^{[L],(i)} \cdot p(\mathbf{y}_{d,t_L}^{[L]} | \mathbf{x}_{d,t_L}^{L,(i)}, \Sigma_{\mathbf{v}_d}^{[L]})$$
  - 27:     **end for**
  - 28: **end for**
  - 29:     Resample particles based on updated weights
  - 30: **end for**
-

## 4 Simulations

In this study, we implement a multiscale switching model to evaluate the dynamics of state transitions across multiple time scales, specifically for  $L = 2$ . The model simulates a scenario involving three state dimensions for  $l = 2$ , three state dimensions for  $l = 1$ , and six individuals, with particle filtering employed to estimate hidden states. The simulation is set up with 100 time steps for  $l = 2$  and 50 time steps for  $l = 1$  per  $l = 2$  step. The initial conditions for the particles are determined by three different starting states for each individual, specifically set to 0.2, 0.5, and 0.7. We use  $N_s = 1,000$  particles. For all simulations, the dimensions of the states for  $l = 1$  and  $l = 2$  are  $N_L = 3$ .

### 4.1 Simulation 1

The true dynamics for  $l = 2$  follow two distinct models over time. In the first third of the simulation (time steps  $t = 1$  to  $t = 33$ ), the true dynamics are governed by model  $m = 0$ , characterized by strong oscillations:

$$\mathbf{x}_{d,t_2}^{[2]} = 3 \sin(\mathbf{x}_{d,t_2-1}^{[2]} + \frac{\pi}{4}) + \left( \frac{\sum_{t_1=1}^{T_1} w_{t_1} \mathbf{x}_{d,t_1}^{[1]}}{\sum_{t_1=1}^{T_1} w_{t_1}} \right) + 0.5 \sum_{d' \neq d} B_{d,d'}^{[2]} \mathbf{x}_{d',t_2-1}^{[2]} + 0.3 \mathbf{A}^{[2]} \mathbf{x}_{d,t_2-1}^{[2]}. \quad (28)$$

In the second third of the simulation (time steps  $t = 34$  to  $t = 66$ ), the dynamics switch to model  $m = 1$  as follows:

$$\mathbf{x}_{d,t_2}^{[2]} = 2 \cos(1.2 \cdot \mathbf{x}_{d,t_2-1}^{[2]}) \cdot \exp(-0.05 \cdot \mathbf{x}_{d,t_2-1}^{[2]}) + \left( \frac{\sum_{t_1=1}^{T_1} w_{t_1} \mathbf{x}_{d,t_1}^{[1]}}{\sum_{t_1=1}^{T_1} w_{t_1}} \right) \quad (29)$$

$$+ \sum_{d' \neq d} B_{d,d'}^{[2]} \mathbf{x}_{d',t_2-1}^{[2]} + 0.5 \mathbf{A}^{[2]} \mathbf{x}_{d,t_2-1}^{[2]}. \quad (30)$$

The dynamics then revert to model  $m = 0$  for the final third of the simulation (time steps  $t = 67$  to  $t = 100$ ). For time scale  $l = 1$ , the dynamics are given by the following equation:

$$\mathbf{x}_{d,t_1}^{[1]} = \cos(1 + \mathbf{A}^{[1]} \mathbf{x}_{d,t_1-1}^{[1]}) + 0.6 \mathbf{x}_{d,t_2-1}^{[2]} \quad (31)$$

Noise is introduced into the models through various covariance matrices. Specifically, the transition noise for  $l = 2$  for each individual  $d$  is defined as follows:  $\Sigma_{\mathbf{w}_{1,t_2}^{[2]}} = 0.5 \mathbf{I}_{N_2}$ ,  $\Sigma_{\mathbf{w}_{2,t_2}^{[2]}} = 0.4 \mathbf{I}_{N_2}$ ,  $\Sigma_{\mathbf{w}_{3,t_2}^{[2]}} = 0.5 \mathbf{I}_{N_2}$ ,  $\Sigma_{\mathbf{w}_{4,t_2}^{[2]}} = 0.7 \mathbf{I}_{N_2}$ ,  $\Sigma_{\mathbf{w}_{5,t_2}^{[2]}} = 0.3 \mathbf{I}_{N_2}$ ,  $\Sigma_{\mathbf{w}_{6,t_2}^{[2]}} = 0.4 \mathbf{I}_{N_2}$ . In contrast, the transition noise for  $l = 1$  is characterized by a lower variance, modeled as  $\Sigma_{\mathbf{w}_d^{[1]}} = 0.05 \mathbf{I}_{N_1}$ . Similarly, the measurement noise for the time scales is specified as follows: for  $l = 2$ , the covariance is given by  $\Sigma_{\mathbf{v}_{d,t_2}^{[2]}} = 0.02 \mathbf{I}_{N_2}$ , while for  $l = 1$ , the measurement noise is represented as  $\Sigma_{\mathbf{v}_{d_1}^{[1]}} = 0.03 \mathbf{I}_{N_1}$ , which is consistent across all individuals. The interaction matrix  $\mathbf{B}^{[2]}$  is initialized as an identity matrix, with one randomly chosen off-diagonal entry set to 1, capturing basic interactions among individuals. Additionally, the adjacency matrix  $\mathbf{A}^{[1]}$  is randomly generated, consisting of zeros and ones to define the interaction structure between dimensions.

#### 4.1.1 Results and Discussion

For all six individuals (Figures 1 through 6), the estimated coarse states generally track the true states well throughout the time series, including during the dynamic transitions between states. In general, our algorithm effectively captures the overall shape and frequency of these oscillations but tends to overshoot or undershoot in some cases, particularly in the first and last third of the time series. Despite these discrepancies, the transitions between different state regimes are well captured, demonstrating the model's capacity to follow the underlying dynamics. The variations in the noise do not have a particularly significant effect on the estimation accuracy. The robustness in capturing the transitions between states highlights the strength of our algorithm, particularly in the more dynamic phases of the time series ( $t_2 = 34, \dots, 66$ ).

The plots for the true vs. estimated model indicators (Figures 1(b) through 6(b)) demonstrate that the switching between model indicators is captured accurately and without delay for all individuals. This is particularly significant as the correct identification of model transitions is crucial for ensuring that the appropriate model is selected at the correct time during the filtering process. The immediate capture of these transitions allows the filter to adapt to changing dynamics swiftly, thereby improving the overall accuracy of state estimation. This timely and accurate switching is especially beneficial in scenarios with nonlinear and complex dynamics, as any delay in detecting a model switch could propagate errors into the state estimates. For some individuals (e.g., Figures 4(b) and 6(b)), there is a slight misalignment with the state estimates.

very beginning of the time series, where the estimated indicator briefly spikes before settling into the correct model. This suggests a potential sensitivity to initial conditions that could be refined with additional prior information or smoothing during initialization. Overall, the accurate capture of transitions for the rest of the time series reflects the robustness of the learning algorithm and demonstrates that it is functioning as intended. The ability to consistently and promptly detect model switches ensures that the filtering process remains efficient and reliable, even in the presence of challenging and abrupt transitions.

The RMSE values for the  $l = 2$  time scale, summarized in Table 2, further quantify the performance of the state estimation across the six individuals and three dimensions. These values reveal that the RMSE is relatively low for all individuals, ranging from approximately 0.111 to 0.157 across the three dimensions. Individuals  $d = 1$  through  $d = 3$  exhibit slightly higher RMSE values compared to Individuals  $d = 4$  through  $d = 6$ , with the highest RMSE being observed for Individual  $d = 3$  in Coarse Dimension 1 at 0.157. Conversely, Individual  $d = 5$  has the lowest overall RMSE across all dimensions, with its Coarse Dimension 3 value reaching as low as 0.111. The differences in RMSE across individuals and dimensions suggest some variability in the estimation performance depending on the specific characteristics of the time series and the noise levels for each individual. Despite this variability, the relatively small range of RMSE values across all individuals indicates that the particle filter maintains a consistent level of accuracy in capturing the coarse states, regardless of the individual’s specific time series dynamics. The robustness in performance, as reflected in these RMSE values, complements the visual analysis of the state trajectories and transitions between model indicators, reinforcing the overall reliability of the algorithm in handling multiscale state estimation. In addition to the results for  $l = 2$ , the RMSE values for time scale  $l = 1$ , presented in Tables 4-24 in the Appendix, indicate a consistent and accurate performance across the individuals. This consistency is further illustrated by Figure 7. Given the number of figures, we have selected just one to highlight these findings, as the results are similar across all  $t_2 = 1, \dots, 100$ .

Individual	Dim 1	Dim 2	Dim 3
Individual $d = 1$	0.125	0.124	0.149
Individual $d = 2$	0.150	0.151	0.153
Individual $d = 3$	0.157	0.150	0.156
Individual $d = 4$	0.149	0.162	0.155
Individual $d = 5$	0.135	0.136	0.111
Individual $d = 6$	0.131	0.129	0.147

Table 2: RMSE values for  $l = 2$  time scale across the three dimensions for each individual.

## 4.2 Simulation 2

For the second set of simulations, the true dynamics for  $l = 2$  follow individual-specific switching patterns, where each individual  $d$  alternates between two models,  $m = 0$  and  $m = 1$ , at different points in time. For  $d = 1$ , the dynamics follow model  $m = 1$  during the first third of the simulation (time steps  $t = 1$  to  $t = 33$ ), model  $m = 0$  in the second third (time steps  $t = 34$  to  $t = 66$ ), and return to model  $m = 1$  in the final third (time steps  $t = 67$  to  $t = 100$ ). Individual  $d = 2$  follows a different pattern, starting with model  $m = 0$  for the first third, switching to model  $m = 1$  for the second third, and then returning to model  $m = 0$  in the final third. Individual  $d = 3$  starts with model  $m = 0$ , switches to model  $m = 1$  during the second third, and remains in model  $m = 1$  for the final third. Individual  $d = 4$  follows model  $m = 1$  for both the first and second thirds of the time series, before switching to model  $m = 0$  in the final third. Individual  $d = 5$  remains in model  $m = 0$  during the first two-thirds of the simulation, switching to model  $m = 1$  only in the final third. Lastly, Individual  $d = 6$  starts with model  $m = 1$ , switches to model  $m = 0$  for the second third, and remains in model  $m = 0$  for the final third.

### 4.2.1 Results and Discussion

In this section, we evaluate the performance of the proposed model for six different individuals by comparing the true states and the estimated states for each individual, as well as the accuracy of the estimated model indicators. Figures 8(a) to 13(a) display the true and estimated states for all dimensions of individuals  $d = 1$  to  $d = 6$ . The figures reveal that, overall, the particle filter accurately tracks the true coarse-scale states, with only minor discrepancies occurring in some individuals during transitions between dynamic regimes. Because the fine time scale state estimates and RMSE results for Simulation 2 are very similar to those for Simulation 1, we have omitted the full set of results and present only one figure to demonstrate the model’s performance. This representative figure (Figure 14) highlights the consistency in the model’s ability to estimate fine time scale states accurately across different simulations.

For  $d = 1$  (Figure 8(a)), the estimated states closely match the true states, with some minor deviations visible during the transitions between models around  $t = 33$  and  $t = 66$ , but the filter quickly recovers and follows the true dynamics well. Next,  $d = 2$  (Figure 9(a)) shows excellent alignment between the true and estimated states. The filter manages to capture the rapid transitions between models at  $t = 33$  and  $t = 66$  accurately, reflecting the capability of the model to adapt to abrupt changes in dynamics. In the case of  $d = 3$  (Figure 10(a)), the estimated states again show close alignment with the true states, with the filter accurately capturing both the oscillatory dynamics and the transitions between models. Individuals  $d = 4$  (Figure 11(a)),  $d = 5$  (Figure 12(a)), and  $d = 6$  (Figure 13(a)) all exhibit similar behavior, with the particle filter accurately estimating the coarse states. Although some minor errors are observed during rapid transitions in  $d = 4$  and  $d = 6$ , these errors are quickly corrected by the model, resulting in good overall performance. Table 3 presents the RMSE values for each individual across the three coarse-scale dimensions. The values indicate that, overall, the particle filter provides accurate state estimates across all dimensions and individuals, with RMSE values remaining relatively low and consistent. Individuals  $d = 1$ ,  $d = 4$ , and  $d = 5$  show the lowest RMSE values, suggesting that the filter performed particularly well for these individuals. In contrast,  $d = 3$  and  $d = 6$  have slightly higher RMSE values, which may reflect the challenges the filter faced in capturing rapid transitions in their dynamic regimes. Despite these small variations, the results confirm the model’s robustness in estimating the coarse-scale states for all individuals.

Figures 8(b) to 13(b) show the true and estimated model indicators for individuals  $d = 1$  to  $d = 6$ . These figures highlight the model’s ability to correctly infer the underlying dynamic model that each individual follows over time. For  $d = 1$  (Figure 8(b)), the estimated indicators align closely with the true indicators, except for a brief discrepancy around  $t = 70$ , where the filter temporarily assigns the wrong model before correcting itself. Despite this, the filter demonstrates high accuracy overall. Individuals  $d = 2$  (Figure 9(b)) and  $d = 3$  show strong alignment between the estimated and true indicators, demonstrating the model’s ability to handle rapid transitions between models effectively. No significant deviations are observed. For  $d = 4$  (Figure 11(b)), a few errors are observed around  $t_2 = 60$  and shortly after  $t_2 = 70$ . However, these errors are temporary, and the model eventually converges to the correct indicator. As well, the transition between the models is accurately estimated. For  $d = 5$  (Figure 12(b)), the estimated indicators show close alignment with the true indicators, with only brief discrepancy in the beginning of the time series that is quickly corrected. However, for individual  $d = 6$  (Figure 13(b)), the model encounters more significant difficulties in detecting the transitions. Around  $t_2 = 30$ , the estimated indicators rapidly oscillate between models before settling into the correct indicator after several time steps. This suggests that while the model is capable of eventually identifying the correct dynamics, it struggles with rapid changes in the underlying model, leading to transient errors in the model indicators during periods of transition. Despite these issues, the model ultimately converges to the correct state.

The results indicate that our proposed learning approach performs well in estimating both the fine and coarse-scale states and the model indicators for all individuals. While some minor discrepancies are observed during periods of rapid transition between models, the filter is generally able to recover and follow the true dynamics accurately. The model is particularly effective in estimating the correct model indicators, with only brief errors occurring in a few individuals.

Individual	Dim 1	Dim 2	Dim 3
Individual $d = 1$	0.134	0.133	0.142
Individual $d = 2$	0.153	0.157	0.146
Individual $d = 3$	0.165	0.146	0.170
Individual $d = 4$	0.139	0.143	0.159
Individual $d = 5$	0.138	0.129	0.126
Individual $d = 6$	0.152	0.143	0.164

Table 3: RMSE values for  $l = 2$  time scale across the three dimensions for each individual.

### 4.3 Conclusion

The multiscale state-space modeling framework developed in this work offers a novel and versatile approach for capturing the dynamics of complex systems. A key innovation of this framework is its ability to model nested nonlinear dynamics, where processes at different levels interact and influence each other. By effectively modeling interactions between different scales, the framework offers a powerful tool for understanding systems with intricate, layered dynamics, where both gradual evolutions and abrupt transitions are critical.

The results demonstrate that our Bayesian learning model, based on this multiscale framework, successfully tracks states and identifies the correct model indicators across all individuals with little variation. The accuracy observed in both state estimates and model indicators highlights the robustness of the framework's switching mechanism, which can handle diverse dynamic regimes. This ability to learn transitions in dynamics is essential for managing complex systems, as these shifts can lead to significant and often irreversible changes in behavior.

Moving forward, a key direction for future work is the integration of nonparametric approaches, such as Dirichlet and Gaussian process priors, to allow for a more flexible model selection process. By utilizing nonparametric methods, we can remove the assumption of a fixed number of known models and enable the model to adaptively discover the appropriate number of dynamic regimes. This could further enhance our framework's ability to capture complex, evolving dynamics, particularly in systems where the number of underlying states or models is unknown or variable.

## References

- [1] M. Sanjeev Arulampalam, Simon Maskell, Neil Gordon, and Tim Clapp. A tutorial on particle filters for online nonlinear/non-Gaussian Bayesian tracking. *IEEE Transactions on Signal Processing*, 50(2):174–188, 2002.
- [2] Vasilis Dakos, Stephen R. Carpenter, William A. Brock, Aaron M. Ellison, Vishwesh Guttal, Anthony R. Ives, Sonia Kéfi, Valerie Livina, David A. Seekell, Egbert H. van Nes, et al. Methods for detecting early warnings of critical transitions in time series illustrated using simulated ecological data. *PLoS One*, 7(7):e41010, 2012.
- [3] Andrew Gelman, John B Carlin, Hal S Stern, and Donald B Rubin. Bayesian data analysis. *Chapman and Hall/CRC*, 1995.
- [4] Alan Hastings, Karen C. Abbott, Kim Cuddington, Tessa Francis, Gabriel Gellner, Ying-Cheng Lai, Andrew Morozov, Sergei Petrovskii, Katherine Scranton, and Mary Lou Zeeman. Transient phenomena in ecology. *Science*, 361(6406):eaat6412, 2018.
- [5] Andrew Morozov, Karen Abbott, and Kim Cuddington. Long transients in ecology: Theory and applications. *Physics of Life Reviews*, 32:1–14, 2020.
- [6] Marten Scheffer, Steve Carpenter, Jonathan A. Foley, Carl Folke, and Brian Walker. Catastrophic shifts in ecosystems. *Nature*, 413(6856):591–596, 2001.
- [7] Nayely Vélez-Cruz and Manfred D. Laubichler. Bayesian learning in a nonlinear multiscale state-space model. *arXiv preprint arXiv:2408.06425*, 2024.

## 5 Appendix A: Derivations for Conditional Distributions

We begin with the full joint posterior for the model, which is written as:

$$\prod_{d=1}^D \prod_{m=1}^M \prod_{l=1}^L \prod_{t_l=1}^{T_l} p \left( \mathbf{x}_{d,t_l}^{[l]}, \mathbf{s}_{d,t_L}^{[L]}, \pi_{d,t_L}^{L,(m)} | \mathbf{y}_{d,t_l}^{[l]}, \alpha_m, \Sigma_{\mathbf{w}_{d,t_l}^{[l]}}, \Sigma_{\mathbf{v}_{d,t_l}^{[l]}} \right) \quad (32)$$

Here, the matrices  $\Sigma_{\mathbf{w}_{d,t_l}^{[l]}}$  and  $\Sigma_{\mathbf{v}_{d,t_l}^{[l]}}$  are known and do not have associated probability density functions. The term  $s_{d,t_L}^{[L]}$  represents the indicator for the model, and  $\pi_{d,t_L}^{L,(m)}$  represents the probabilities associated with selecting the indicators.

### 5.1 Conditional Posterior of the Model Probabilities $\pi_{d,t_L}^{[L]}$

The full conditional for the model probabilities  $\pi_{d,t_L}^{[L]}$  can be derived by considering the joint posterior and applying Bayes' theorem. We take into account the number of times each indicator  $s_{d,t_L}^{[L]}$  was selected. The posterior depends on both the prior for  $\pi_{d,t_L}^{[L]}$  (a Dirichlet distribution) and the categorical distribution for  $s_{d,t_L}^{[L]}$ , which is conditional on the previous indicators  $\mathcal{S}_{d,t_L-1}^{[L]}$  and the probabilities  $\pi_{d,t_L}^{[L]}$ . We write the full conditional posterior for  $\pi_{d,t_L}^{[L]}$  as follows:

$$p(\pi_{d,t_L}^{[L]} | \mathbf{s}_{d,t_L}^{[L]}, \boldsymbol{\alpha}) \propto p(\mathbf{s}_{d,t_L}^{[L]} | \mathcal{S}_{d,1:t_L-1}^{[L]}, \pi_{d,t_L}^{[L]}) p(\pi_{d,t_L}^{[L]} | \boldsymbol{\alpha}) \quad (33)$$

The indicators  $s_{d,t_L}^{[L]}$  are drawn from a categorical distribution. The probability of selecting a specific model at time  $t_L$  depends on the set of past indicators  $\mathcal{S}_{d,t_L-1}^{[L]}$  for time  $t_L = 1, \dots, t_L - 1$  and the probabilities  $\pi_{d,t_L}^{[L]}$ . The conditional distribution for  $s_{d,t_L}^{[L]}$  is written as:

$$p(s_{d,t_L}^{[L]} | \mathcal{S}_{d,t_L-1}^{[L]}, \pi_{d,t_L}^{[L]}) = \prod_{t_L=1}^{T_L} \text{Cat} \left( s_{d,t_L}^{[L]} | \mathcal{S}_{d,t_L-1}^{[L]}, \pi_{d,t_L}^{[L]} \right) \quad (34)$$

Here,  $s_{d,t_L}^{[L]}$  follows a categorical distribution where the probabilities for selecting each model at time  $t_L$  are given by the vector  $\pi_{d,t_L}^{[L]}$ . The prior on the model probabilities  $\pi_{d,t_L}^{[L]}$  is a Dirichlet distribution with parameters  $\boldsymbol{\alpha} = (\alpha_1, \alpha_2, \dots, \alpha_M)$ , encoding the prior belief about how likely each model is to be selected:

$$p(\pi_{d,t_L}^{[L]} | \boldsymbol{\alpha}) = \text{Dir}(\alpha_1, \alpha_2, \dots, \alpha_M) \quad (35)$$

To derive the full conditional for  $\pi_{d,t_L}^{[L]}$ , we apply Bayes' theorem. By multiplying the probability of the indicators by the prior distribution of  $\pi_{d,t_L}^{[L]}$ , we have:

$$p(\pi_{d,t_L}^{[L]} | \mathbf{s}_{d,t_L}^{[L]}, \boldsymbol{\alpha}) \propto \left( \prod_{t_L=1}^{T_L} \text{Cat} \left( s_{d,t_L}^{[L]} | \mathcal{S}_{d,t_L-1}^{[L]}, \pi_{d,t_L}^{[L]} \right) \right) \text{Dir}(\alpha_1, \alpha_2, \dots, \alpha_M) \quad (36)$$

Because the Dirichlet distribution is conjugate to the categorical distribution, the resulting posterior for  $\pi_{d,t_L}^{[L]}$  is also Dirichlet. The updated parameters of this posterior are the sum of the prior parameters  $\alpha_m$  and the counts  $c_{d,1:t_L-1}^{[L),(m)}$ , where  $c_{d,1:t_L-1}^{[L),(m)}$  is the number of times the indicator  $s_{d,t_L}^{[L]} = m$  has been observed up to time  $t_L - 1$ . Thus, the full conditional is:

$$\pi_{d,t_L}^{[L]} | \mathcal{S}_{d,t_L-1}^{[L]}, \mathbf{s}_{d,t_L}^{[L]} \sim \text{Dir} \left( \alpha_1 + c_{d,1:t_L-1}^{[L),(1)}, \alpha_2 + c_{d,1:t_L-1}^{[L),(2)}, \dots, \alpha_M + c_{d,1:t_L-1}^{[L),(M)} \right) \quad (37)$$

### 5.2 Conditional Posterior of the Model Indicators $s_{d,t_L}^{[L]}$

Next, we derive the conditional posterior of the indicator  $s_{d,t_L}^{[L]}$ :

$$p(s_{d,t_L}^{[L]} | \mathcal{S}_{d,t_L-1}^{[L]}, \mathbf{x}_{d,t_L}^{[L]}, \mathbf{y}_{d,t_L}^{[L]}, \pi_{d,t_L}^{L,(m)}), \quad (38)$$

Recall, the joint posterior for all unknowns, including states, indicators, and probabilities, is given by:

$$\prod_{d=1}^D \prod_{m=1}^M \prod_{l=1}^L \prod_{t_l=1}^{T_l} p \left( \mathbf{x}_{d,t_l}^{[l]}, \mathbf{s}_{d,t_l}^{[L]}, \pi_{d,t_l}^{L,(m)} | \mathbf{y}_{d,t_l}^{[l]}, \alpha_m, \Sigma_{\mathbf{w}_{d,t_l}^{[l]}}, \Sigma_{\mathbf{v}_{d,t_l}^{[l]}} \right) \quad (39)$$

where for brevity we have omitted the measurement and process noise covariance matrices as they are assumed to be known. Since the indicators  $\mathbf{s}_{d,t_L}^{[L]}$  only affect the coarse time scale  $L$ , we can factor the joint posterior recursively by time steps  $T_L$ . For each time step  $t_L$ , and using the Markov assumption to factor recursively, the joint posterior can be written as:

$$p(\mathbf{x}_{d,1:T_L}^{[L]}, \left\{ \mathbf{x}_{d,1:T_{l'}}^{[l']} \right\}_{l'=1}^{L-1}, \mathbf{s}_{d,1:T_L}^{[L]}, \pi_{d,1:T_L}^{[L]} | \mathbf{y}_{d,t_L}^{[L]}, \boldsymbol{\alpha}) \quad (40)$$

$$= p(\mathbf{x}_{d,t_L}^{[L]}, \left\{ \mathbf{x}_{d,1:T_{l'}}^{[l']} \right\}_{l'=1}^{L-1}, \mathbf{s}_{d,t_L}^{[L]}, \pi_{d,t_L}^{[L]} | \mathbf{y}_{d,1:t_L}^{[L]}, \mathbf{x}_{1:t_L-1}^{[L]}, \mathcal{S}_{d,t_L-1}^{[L]}, \pi_{d,1:t_L-1}^{[L]}, \boldsymbol{\alpha}) \quad (41)$$

$$p(\mathbf{x}_{d,1:t_L-1}^{[L]}, \mathcal{S}_{d,t_L-1}^{[L]}, \pi_{d,1:t_L-1}^{[L]} | \mathbf{y}_{d,1:t_L-1}^{[L]}) \quad (42)$$

In practice, during the particle filter update step, the joint posterior up to the previous time step  $t_{L-1}$  is taken into account. This means that the term

$$p(\mathbf{x}_{d,1:t_L-1}^{[L]}, \mathcal{S}_{d,t_L-1}^{[L]}, \pi_{d,1:t_L-1}^{[L]} | \mathbf{y}_{d,1:t_L-1}^{[L]})$$

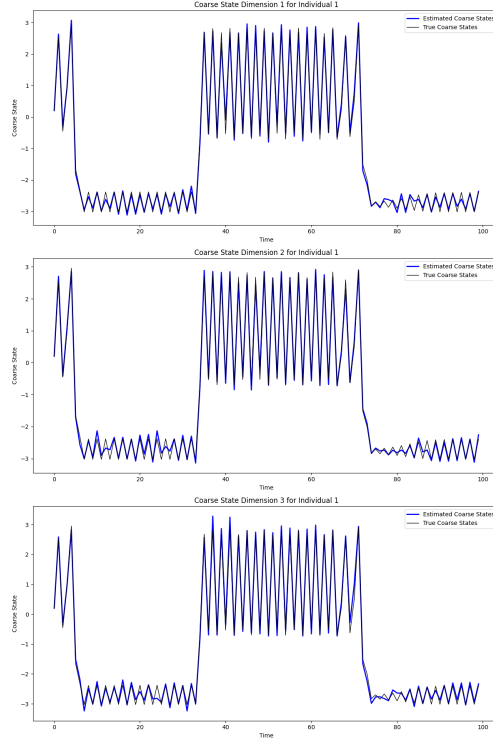
represents the contribution of the previous time steps and is recursively updated using particle filtering. As new observations come in, the particle filter updates the posterior at the current time step  $t_L$  based on the filtered states and indicators from the previous time step. Using Bayes' theorem, the conditional posterior can be factored as follows:

$$p(s_{d,t_L}^{[L]} | \mathcal{S}_{d,t_L-1}^{[L]}, \mathbf{x}_{d,t_L}^{[L]}, \mathbf{y}_{d,t_L}^{[L]}, \pi_{d,t_L}^{L,(m)}) \propto p(\mathbf{y}_{d,t_L}^{[L]} | \mathbf{x}_{d,t_L}^{[L]}) \\ p(\mathbf{x}_{d,t_L}^{[L]} | s_{d,t_L}^{[L]}, \mathbf{x}_{d,t_L-1}^{[L]}, \left\{ \mathbf{x}_{d,1:T_{l'}}^{[l']} \right\}_{l'=1}^{L-1}) p(s_{d,t_L}^{[L]} | \mathcal{S}_{d,t_L-1}^{[L]}, \pi_{d,t_L}^{L,(m)}) \quad (43)$$

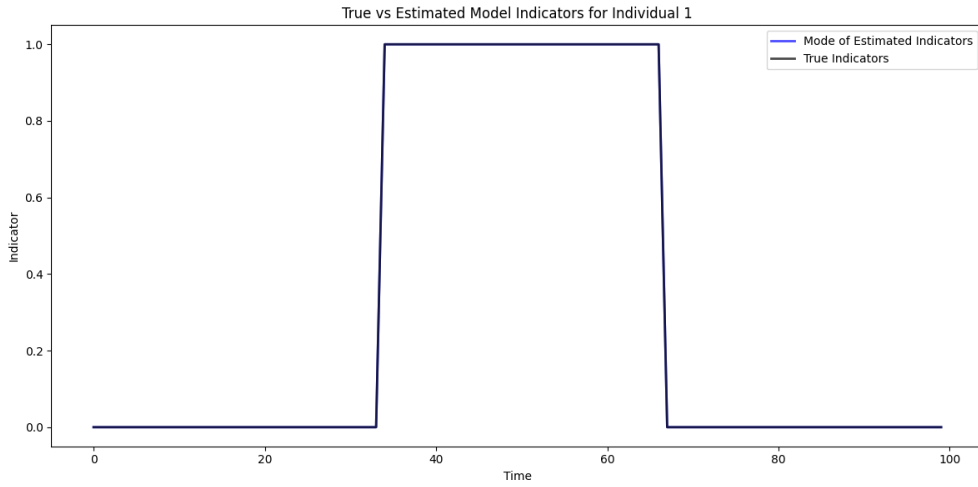
The first term in this factorization is the likelihood. The second term is the state transition model, which describes how the current state  $\mathbf{x}_{d,t_L}^{[L]}$  evolves from the previous state  $\mathbf{x}_{d,t_L-1}^{[L]}$ , and is influenced by the finer time scale states  $\left\{ \mathbf{x}_{d,1:T_{l'}}^{[l']} \right\}_{l'=1}^{L-1}$  and the indicator  $s_{d,t_L}^{[L]}$  corresponding to model  $m$ . The third term is the prior on the indicator  $s_{d,t_L}^{[L]}$ , which depends on the previous indicators  $\mathcal{S}_{d,t_L-1}^{[L]}$  and the probabilities  $\pi_{d,t_L}^{L,(m)}$ :

$$p(s_{d,t_L}^{[L]} | \mathcal{S}_{d,t_L-1}^{[L]}, \mathbf{x}_{d,t_L}^{[L]}, \mathbf{y}_{d,t_L}^{[L]}, \pi_{d,t_L}^{L,(m)}) \propto p(\mathbf{y}_{d,t_L}^{[L]} | \mathbf{x}_{d,t_L}^{[L]}) \\ p(\mathbf{x}_{d,t_L}^{[L]} | s_{d,t_L}^{[L]}, \mathbf{x}_{d,t_L-1}^{[L]}, \left\{ \mathbf{x}_{d,1:T_{l'}}^{[l']} \right\}_{l'=1}^{L-1}) \\ p(s_{d,t_L}^{[L]} | \mathcal{S}_{d,t_L-1}^{[L]}, \pi_{d,t_L}^{L,(m)}) \quad (44)$$

5.3 Figures

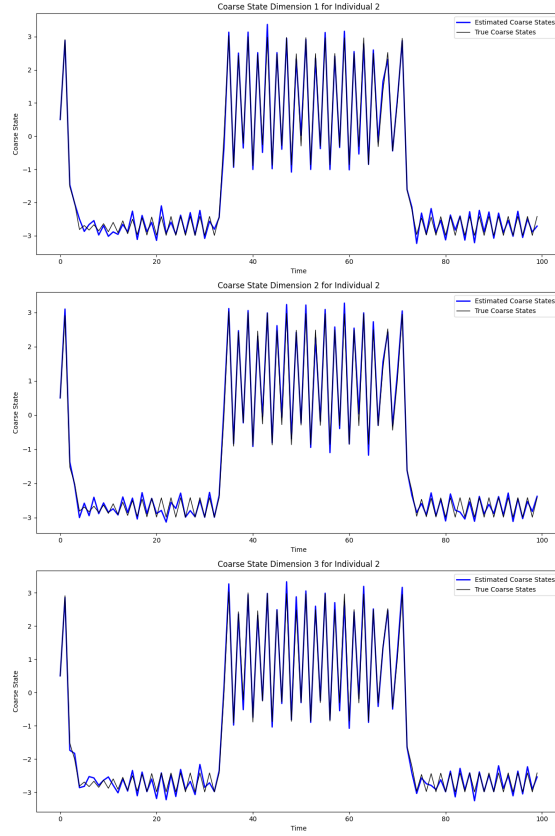


(a) Individual 1: State Estimate with  $\Sigma_{\mathbf{w}_{1,t_2}^{[2]}} = 0.5 \mathbf{I}_{N_2}$

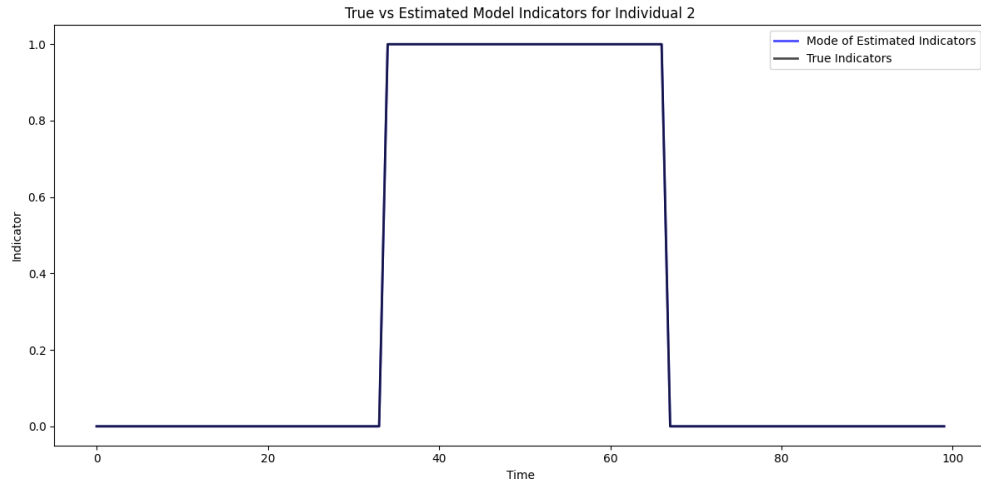


(b) Individual 1: True vs. Estimated Indicator with  $\Sigma_{\mathbf{w}_{1,t_2}^{[2]}} = 0.5 \mathbf{I}_{N_2}$

Figure 1: Comparison of true states and estimated states for Individual 1, along with the estimated indicator. In the indicator plot, blue indicates the estimated model indicator while black represents the true model indicator.

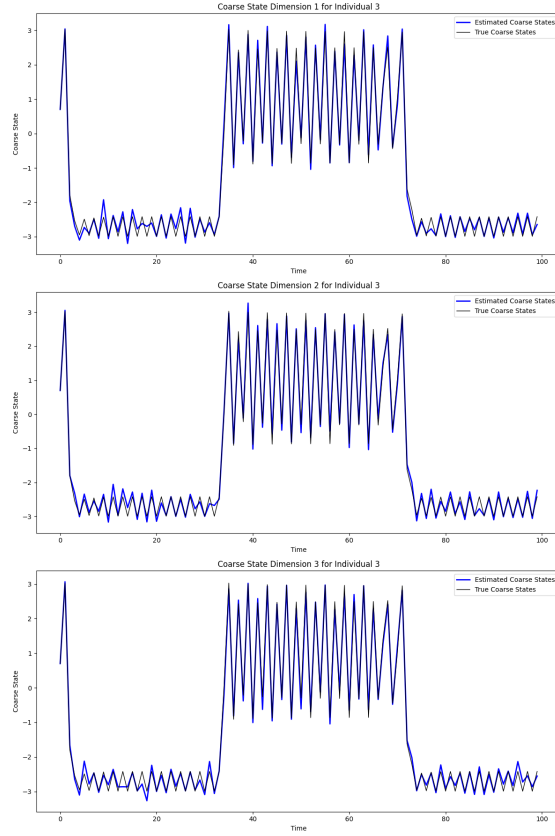


(a) Individual 2: State Estimate with  $\Sigma_{\mathbf{w}_{2,t_2}^{[2]}} = 0.4 \mathbf{I}_{N_2}$

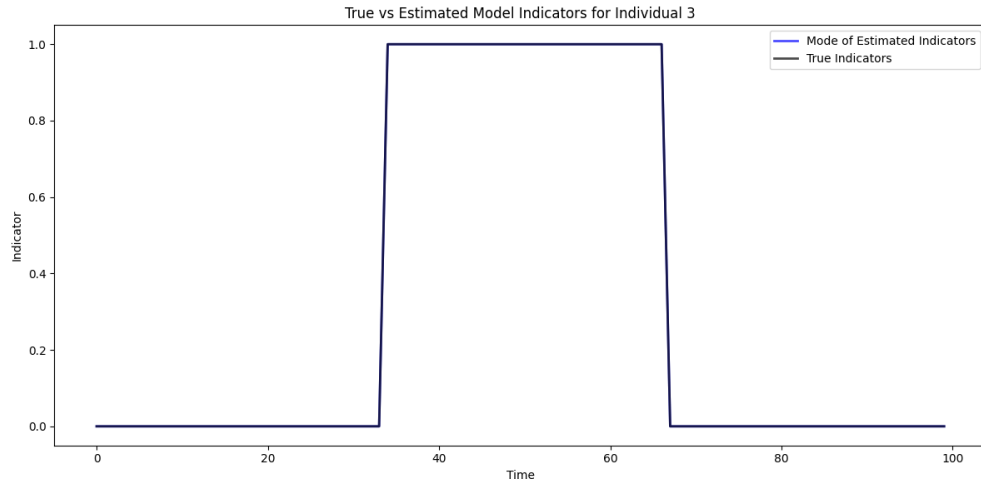


(b) Individual 2: True vs. Estimated Indicator with  $\Sigma_{\mathbf{w}_{2,t_2}^{[2]}} = 0.4 \mathbf{I}_{N_2}$

Figure 2: Comparison of true states and estimated states for Individual 2, along with the estimated indicator. In the indicator plot, blue indicates the estimated model indicator while black represents the true model indicator.

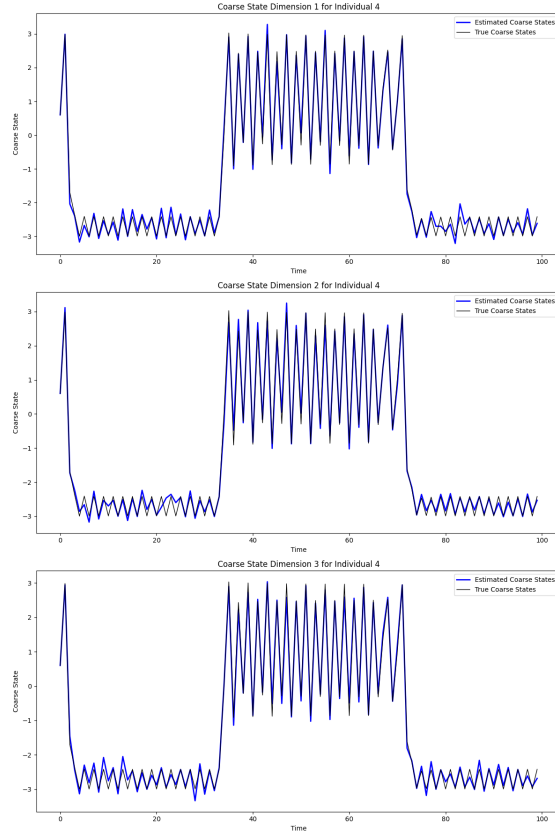


(a) Individual 3: State Estimate with  $\Sigma_{\mathbf{w}_{3,t_2}^{[2]}} = 0.5 \mathbf{I}_{N_2}$

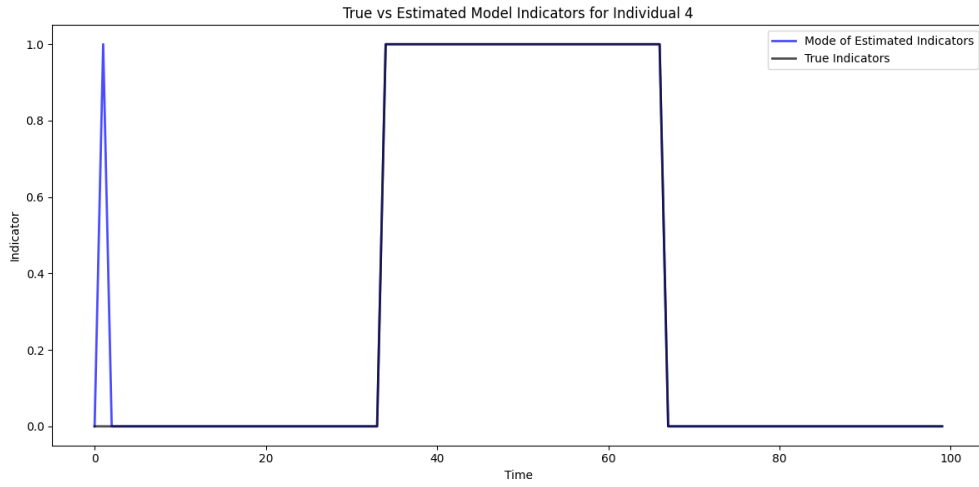


(b) Individual 3: True vs. Estimated Indicator with  $\Sigma_{\mathbf{w}_{3,t_2}^{[2]}} = 0.5 \mathbf{I}_{N_2}$

Figure 3: Comparison of true states and estimated states for Individual 3, along with the estimated indicator. In the indicator plot, blue indicates the estimated model indicator while black represents the true model indicator.

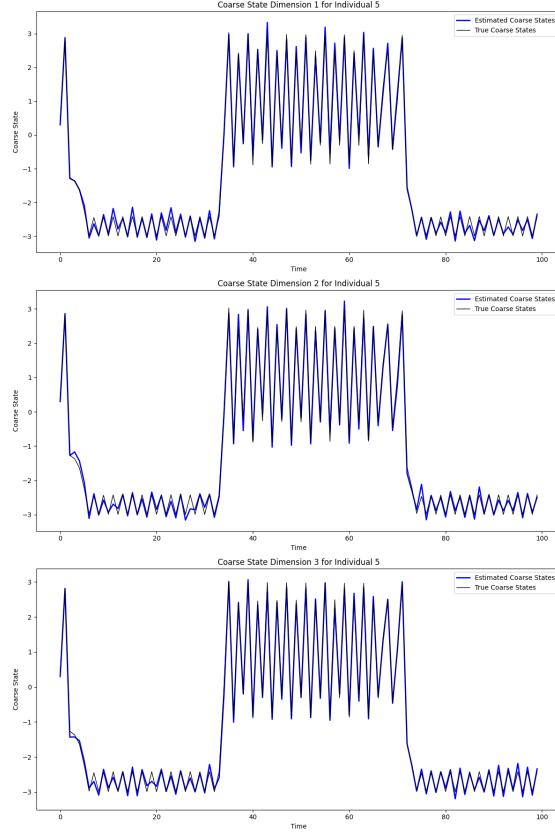


(a) Individual 4: State Estimate with  $\Sigma_{\mathbf{w}_{4,t_2}^{[2]}} = 0.7 \mathbf{I}_{N_2}$

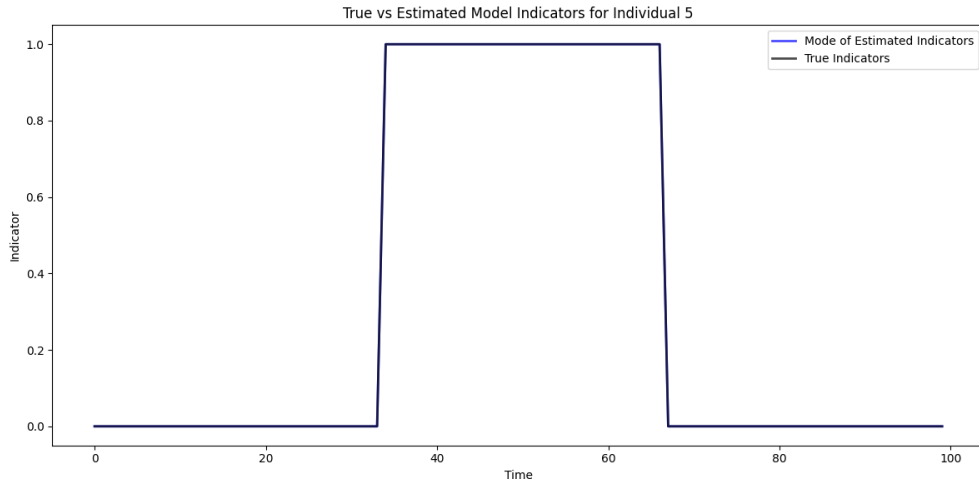


(b) Individual 4: True vs. Estimated Indicator with  $\Sigma_{\mathbf{w}_{4,t_2}^{[2]}} = 0.7 \mathbf{I}_{N_2}$

Figure 4: Comparison of true states and estimated states for Individual 4, along with the estimated indicator. In the indicator plot, blue indicates the estimated model indicator while black represents the true model indicator.

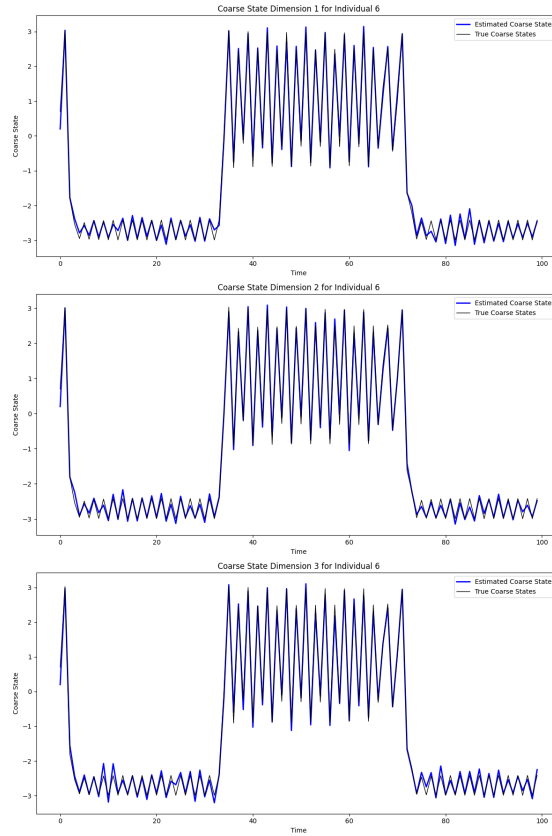


(a) Individual 5: State Estimate with  $\Sigma_{\mathbf{w}_{5,t_2}^{[2]}} = 0.3 \mathbf{I}_{N_2}$

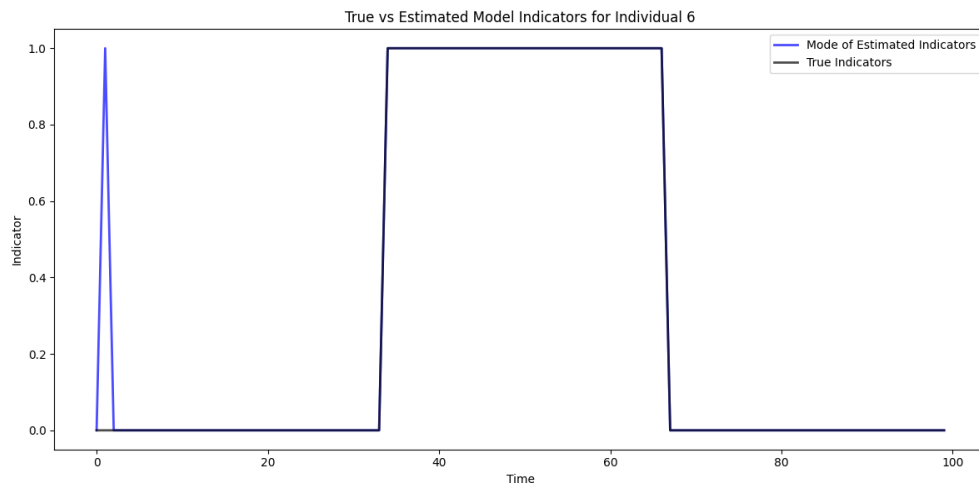


(b) Individual 5: True vs. Estimated Indicator with  $\Sigma_{\mathbf{w}_{5,t_2}^{[2]}} = 0.3 \mathbf{I}_{N_2}$

Figure 5: Comparison of true states and estimated states for Individual 5, along with the estimated indicator. In the indicator plot, blue indicates the estimated model indicator while black represents the true model indicator.



(a) Individual 6: State Estimate with  $\Sigma_{\mathbf{w}_{6,t_2}^{[2]}} = 0.4 \mathbf{I}_{N_2}$



(b) Individual 6: True vs. Estimated Indicator with  $\Sigma_{\mathbf{w}_{6,t_2}^{[2]}} = 0.4 \mathbf{I}_{N_2}$

Figure 6: Comparison of true states and estimated states for Individual 6, along with the estimated indicator. In the indicator plot, blue indicates the estimated model indicator while black represents the true model indicator.

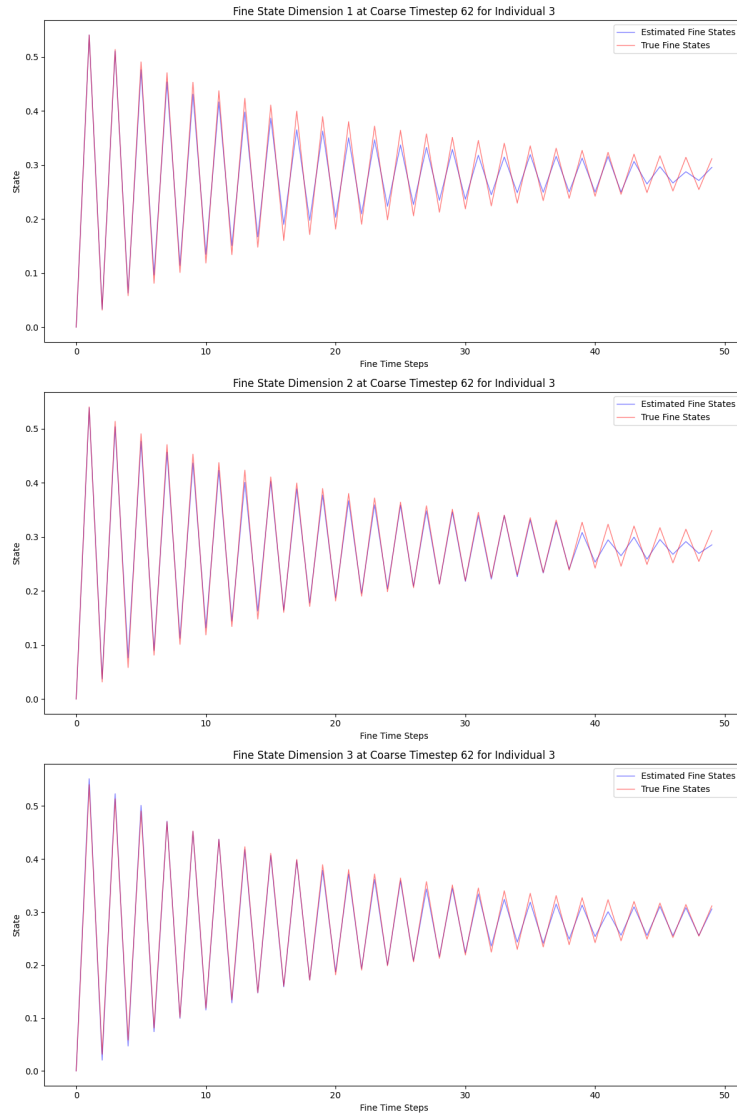
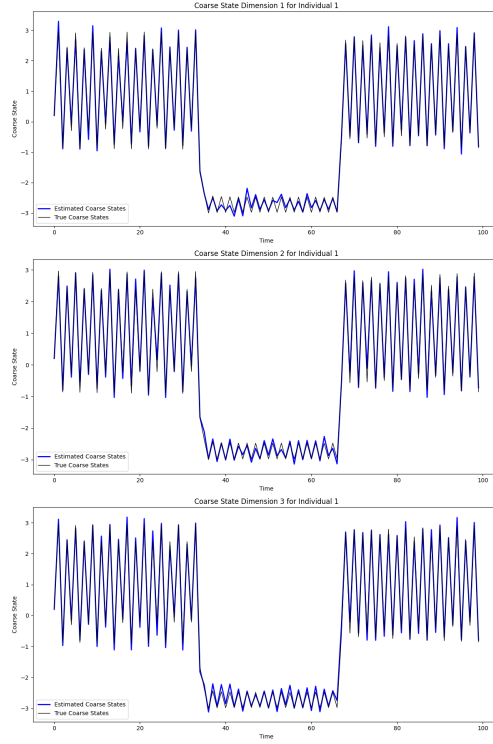
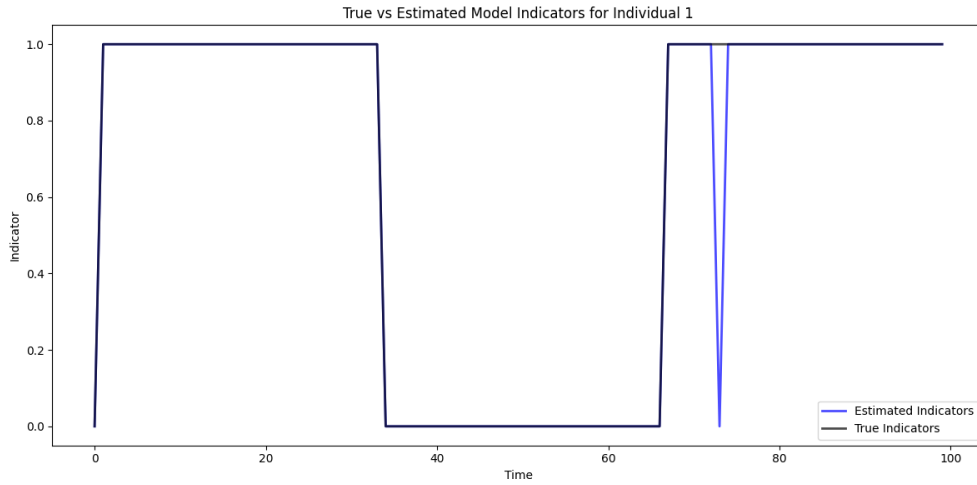


Figure 7: Comparison of true states and estimated states for Individual 3 at  $t_2 = 62$

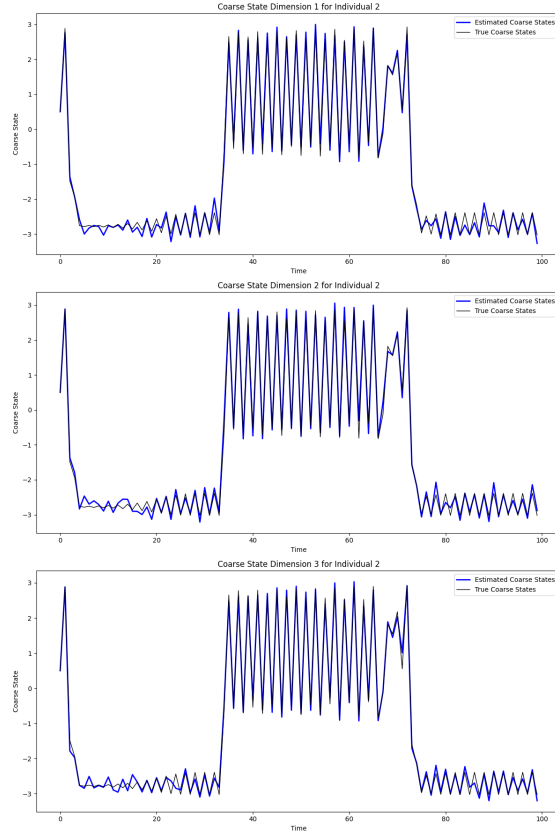


(a) Individual 1: State Estimate with  $\Sigma_{\mathbf{w}_{1,t_2}^{[2]}} = 0.5 \mathbf{I}_{N_2}$

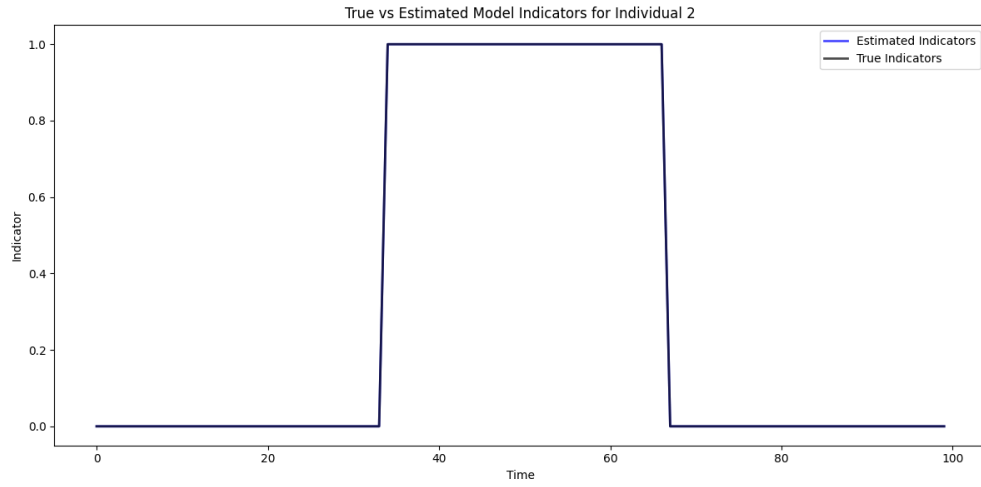


(b) Individual 1: True vs. Estimated Indicator with  $\Sigma_{\mathbf{w}_{1,t_2}^{[2]}} = 0.5 \mathbf{I}_{N_2}$

Figure 8: Comparison of true states and estimated states for Individual 1 (Simulation 2), along with the estimated indicator. In the indicator plot, blue indicates the estimated model indicator while black represents the true model indicator.

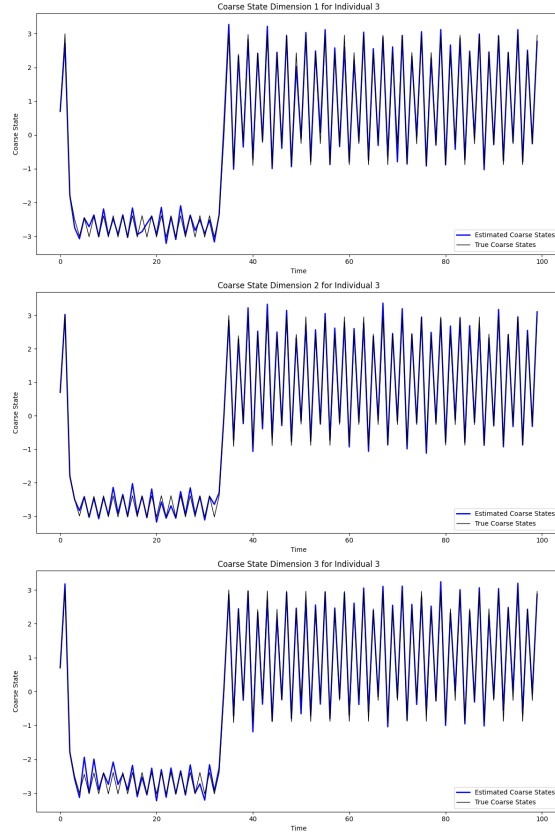


(a) Individual 2: State Estimate with  $\Sigma_{\mathbf{w}_{2,t_2}^{[2]}} = 0.4 \mathbf{I}_{N_2}$

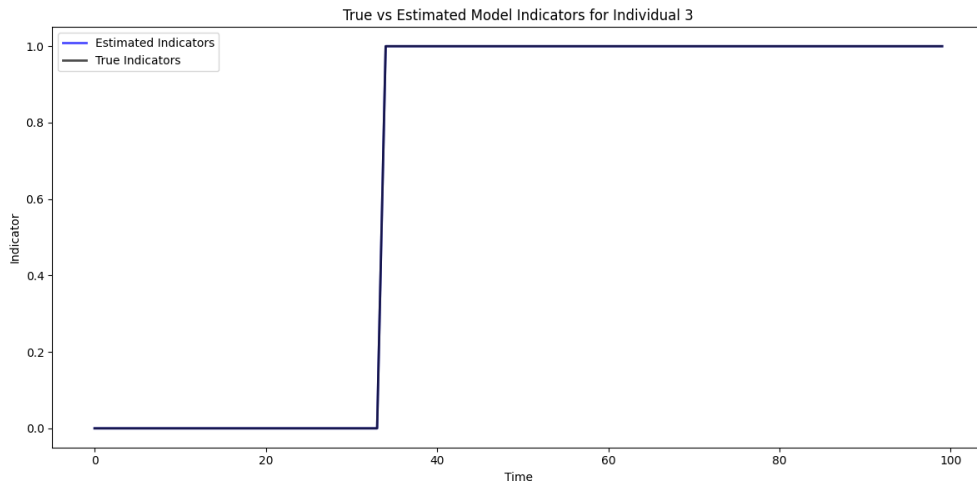


(b) Individual 2: True vs. Estimated Indicator with  $\Sigma_{\mathbf{w}_{2,t_2}^{[2]}} = 0.4 \mathbf{I}_{N_2}$

Figure 9: Comparison of true states and estimated states for Individual 2 (Simulation 2), along with the estimated indicator. In the indicator plot, blue indicates the estimated model indicator while black represents the true model indicator.

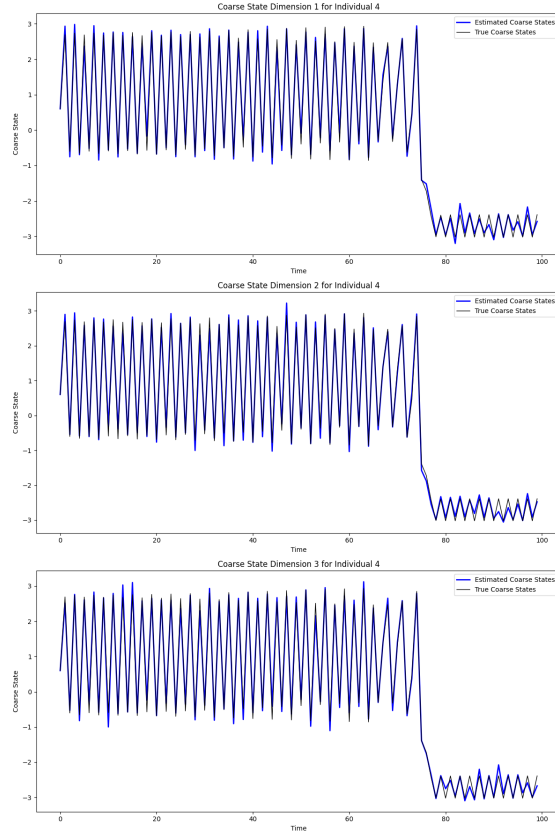


(a) Individual 3: State Estimate with  $\Sigma_{\mathbf{w}_{3,t_2}^{[2]}} = 0.5 \mathbf{I}_{N_2}$

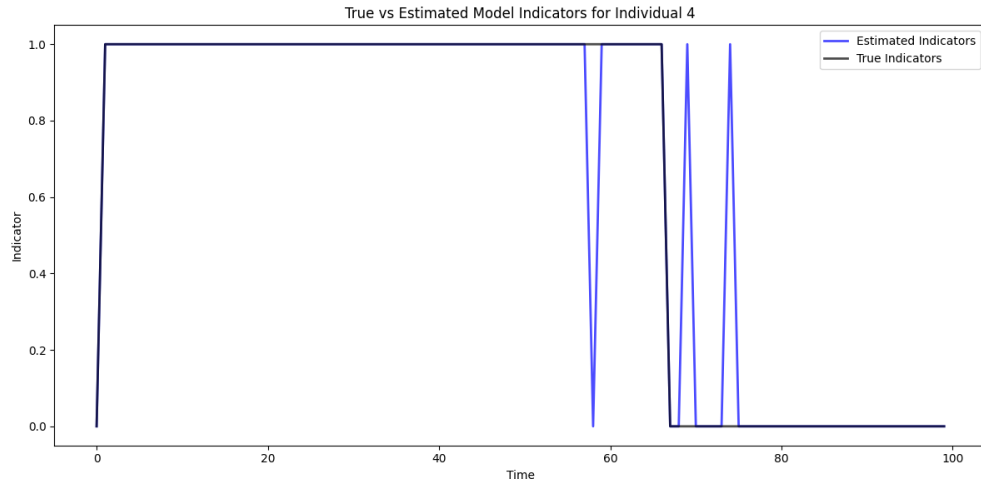


(b) Individual 3: True vs. Estimated Indicator with  $\Sigma_{\mathbf{w}_{3,t_2}^{[2]}} = 0.5 \mathbf{I}_{N_2}$

Figure 10: Comparison of true states and estimated states for Individual 3 (Simulation 2), along with the estimated indicator. In the indicator plot, blue indicates the estimated model indicator while black represents the true model indicator.

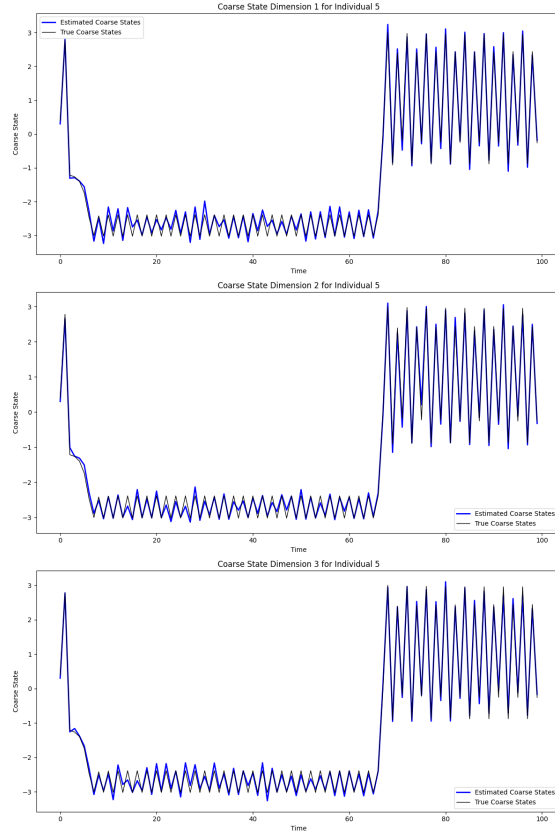


(a) Individual 4: State Estimate with  $\Sigma_{\mathbf{w}_{4,t_2}^{[2]}} = 0.7 \mathbf{I}_{N_2}$

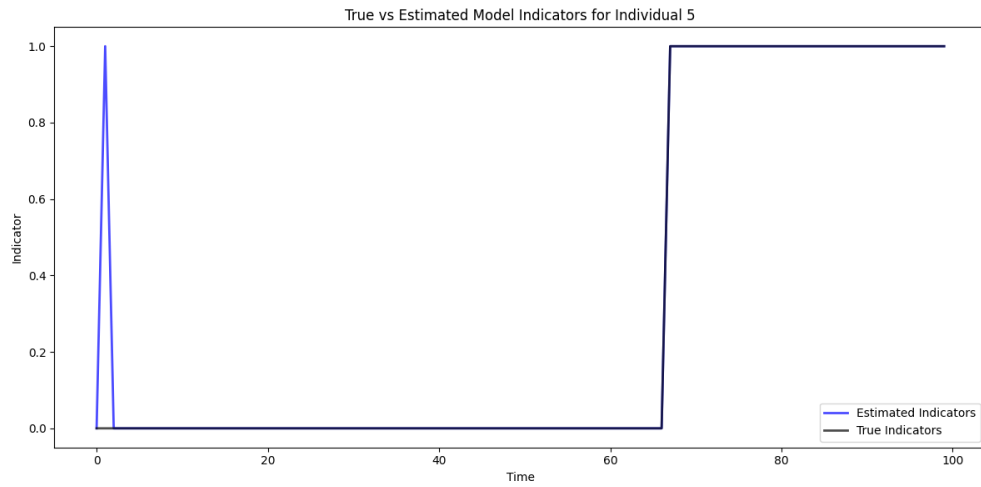


(b) Individual 4: True vs. Estimated Indicator with  $\Sigma_{\mathbf{w}_{4,t_2}^{[2]}} = 0.7 \mathbf{I}_{N_2}$

Figure 11: Comparison of true states and estimated states for Individual 4 (Simulation 2), along with the estimated indicator. In the indicator plot, blue indicates the estimated model indicator while black represents the true model indicator.

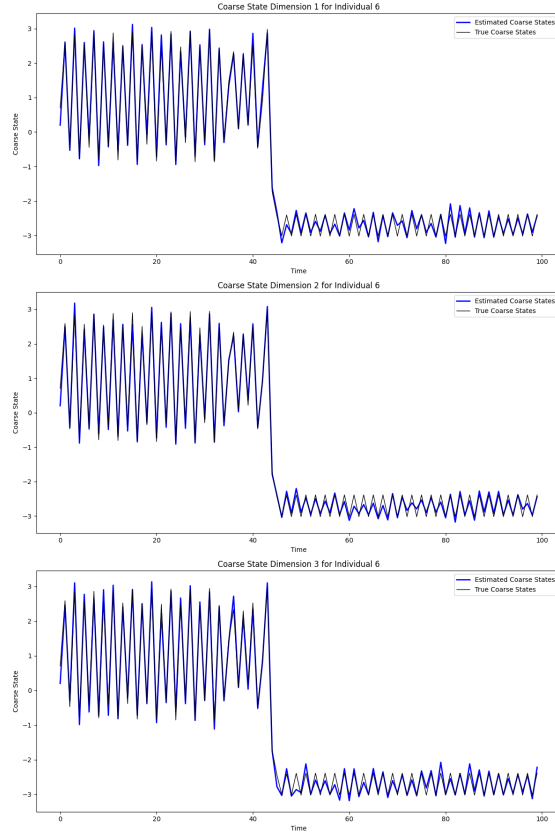


(a) Individual 5: State Estimate with  $\Sigma_{\mathbf{w}_{5,t_2}^{[2]}} = 0.3 \mathbf{I}_{N_2}$

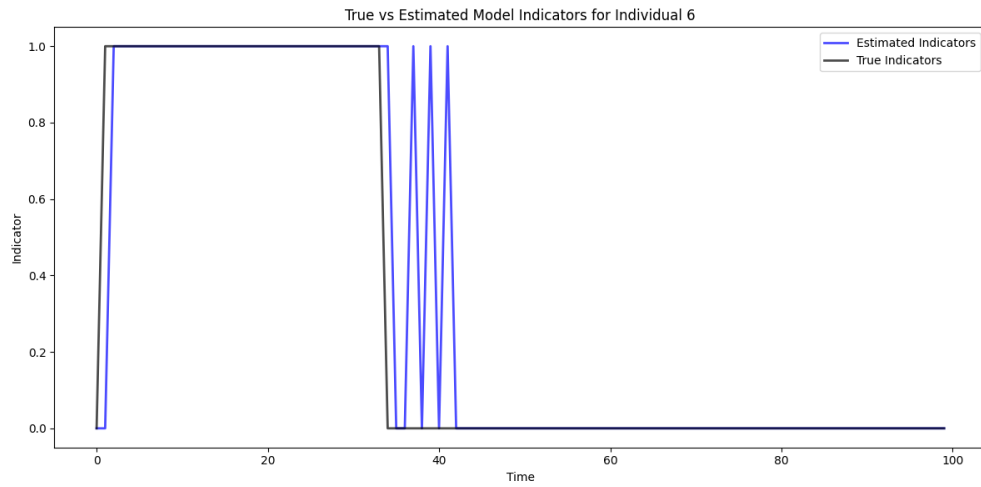


(b) Individual 5: True vs. Estimated Indicator with  $\Sigma_{\mathbf{w}_{5,t_2}^{[2]}} = 0.3 \mathbf{I}_{N_2}$

Figure 12: Comparison of true states and estimated states for Individual 5 (Simulation 2), along with the estimated indicator. In the indicator plot, blue indicates the estimated model indicator while black represents the true model indicator.



(a) Individual 6: State Estimate with  $\Sigma_{\mathbf{w}_{\delta, t_2}^{[2]}} = 0.4 \mathbf{I}_{N_2}$



(b) Individual 6: True vs. Estimated Indicator with  $\Sigma_{\mathbf{w}_{\delta, t_2}^{[2]}} = 0.4 \mathbf{I}_{N_2}$

Figure 13: Comparison of true states and estimated states for Individual 6 (Simulation 2), along with the estimated indicator. In the indicator plot, blue indicates the estimated model indicator while black represents the true model indicator.

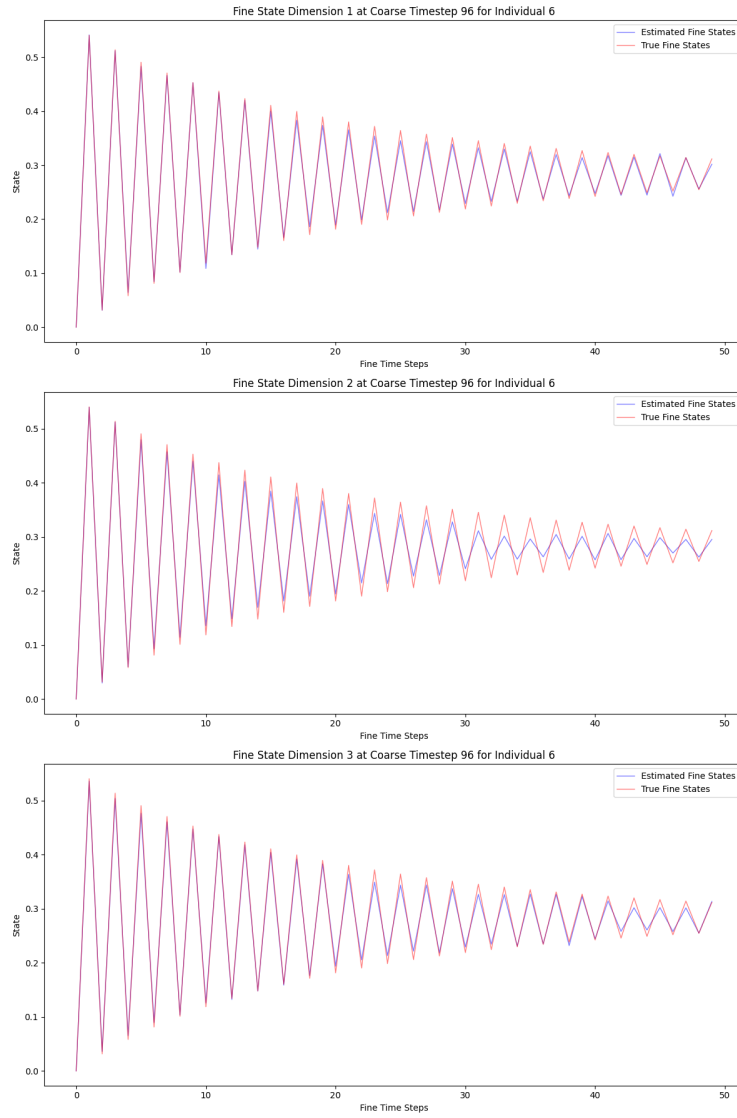


Figure 14: Comparison of true states and estimated states for Individual 3 at  $t_2 = 96$  (Simulation 2)

Individual	Coarse Step 1			Coarse Step 2			Coarse Step 3			Coarse Step 4			Coarse Step 5		
	Dim 1	Dim 2	Dim 3	Dim 1	Dim 2	Dim 3	Dim 1	Dim 2	Dim 3	Dim 1	Dim 2	Dim 3	Dim 1	Dim 2	Dim 3
Individual 1	2.75e-16	2.75e-16	2.75e-16	0.123	0.0899	0.0931	0.0236	0.0208	0.0196	0.118	0.101	0.0752	0.0156	0.0141	0.0166
Individual 2	2.75e-16	2.75e-16	2.75e-16	0.0806	0.105	0.0794	0.00999	0.0247	0.022	0.0677	0.0996	0.112	0.0111	0.0229	0.0198
Individual 3	2.75e-16	2.75e-16	2.75e-16	0.0984	0.0952	0.143	0.0218	0.0272	0.0245	0.0813	0.107	0.0922	0.0176	0.0236	0.0182
Individual 4	2.75e-16	2.75e-16	2.75e-16	0.0947	0.125	0.0917	0.0109	0.0272	0.0227	0.0804	0.112	0.109	0.0228	0.0139	0.0187
Individual 5	2.75e-16	2.75e-16	2.75e-16	0.0602	0.103	0.0881	0.0146	0.0216	0.00997	0.0998	0.116	0.0928	0.0228	0.0282	0.0121
Individual 6	2.75e-16	2.75e-16	2.75e-16	0.102	0.13	0.0725	0.0234	0.0201	0.0207	0.113	0.0871	0.0868	0.014	0.0141	0.0185

Table 4: Results for Coarse Steps 1 to 5 across dimensions for all individuals

Individual	Coarse Step 6			Coarse Step 7			Coarse Step 8			Coarse Step 9			Coarse Step 10		
	Dim 1	Dim 2	Dim 3	Dim 1	Dim 2	Dim 3	Dim 1	Dim 2	Dim 3	Dim 1	Dim 2	Dim 3	Dim 1	Dim 2	Dim 3
Individual 1	0.0955	0.0681	0.118	0.0214	0.0222	0.0235	0.121	0.0936	0.0816	0.0200	0.0168	0.0229	0.104	0.1029	0.0923
Individual 2	0.1029	0.0823	0.0903	0.0232	0.0239	0.0208	0.0857	0.128	0.0756	0.0306	0.0197	0.0168	0.0899	0.1097	0.0926
Individual 3	0.0838	0.0945	0.100	0.0195	0.0138	0.0185	0.1057	0.1014	0.116	0.0210	0.0093	0.0201	0.1026	0.1388	0.0711
Individual 4	0.108	0.0637	0.0823	0.0203	0.0173	0.0270	0.100	0.0808	0.0845	0.0200	0.0093	0.0243	0.0983	0.111	0.0799
Individual 5	0.0951	0.0807	0.124	0.0176	0.0216	0.0160	0.0834	0.1346	0.0862	0.0245	0.0208	0.0269	0.116	0.1136	0.0864
Individual 6	0.111	0.0910	0.124	0.0303	0.0182	0.0203	0.0833	0.102	0.131	0.0239	0.0162	0.0206	0.0987	0.0844	0.112

Table 5: Results for Coarse Steps 6 to 10 across dimensions for all individuals

Individual	Coarse Step 11			Coarse Step 12			Coarse Step 13			Coarse Step 14			Coarse Step 15		
	Dim 1	Dim 2	Dim 3	Dim 1	Dim 2	Dim 3	Dim 1	Dim 2	Dim 3	Dim 1	Dim 2	Dim 3	Dim 1	Dim 2	Dim 3
Individual 1	0.0267	0.0124	0.0147	0.133	0.0927	0.0863	0.0175	0.0187	0.0291	0.123	0.0939	0.0751	0.0219	0.0227	0.0076
Individual 2	0.0175	0.0233	0.0210	0.0635	0.128	0.101	0.0203	0.0141	0.0336	0.0693	0.0757	0.0965	0.0112	0.0090	0.0160
Individual 3	0.0221	0.0138	0.0082	0.107	0.0996	0.0981	0.0271	0.0178	0.0132	0.104	0.106	0.106	0.0172	0.0258	0.0200
Individual 4	0.0159	0.0085	0.0286	0.0963	0.0909	0.122	0.0085	0.0089	0.0211	0.0806	0.0752	0.0999	0.0150	0.0291	0.0160
Individual 5	0.0174	0.0250	0.0084	0.104	0.100	0.0980	0.0089	0.0239	0.0432	0.0655	0.1157	0.122	0.0289	0.0119	0.0183
Individual 6	0.0132	0.0191	0.0156	0.0821	0.129	0.0705	0.0184	0.0159	0.0188	0.0846	0.1176	0.109	0.0231	0.0129	0.0136

Table 6: Results for Coarse Steps 11 to 15 across dimensions for all individuals

Individual	Coarse Step 16			Coarse Step 17			Coarse Step 18			Coarse Step 19			Coarse Step 20		
	Dim 1	Dim 2	Dim 3	Dim 1	Dim 2	Dim 3	Dim 1	Dim 2	Dim 3	Dim 1	Dim 2	Dim 3	Dim 1	Dim 2	Dim 3
Individual 1	0.119	0.102	0.0840	0.0236	0.0135	0.0339	0.0713	0.110	0.119	0.0250	0.0195	0.0203	0.117	0.102	0.0920
Individual 2	0.0890	0.0863	0.113	0.0195	0.0300	0.0119	0.115	0.101	0.098	0.0202	0.0244	0.0159	0.0768	0.0928	0.116
Individual 3	0.0944	0.0941	0.112	0.0071	0.0122	0.0268	0.0736	0.0851	0.118	0.0276	0.0167	0.0249	0.135	0.104	0.0660
Individual 4	0.118	0.100	0.116	0.0176	0.0239	0.0195	0.0859	0.115	0.0752	0.0203	0.0118	0.0261	0.110	0.101	0.109
Individual 5	0.116	0.0895	0.0930	0.0215	0.0333	0.00915	0.0830	0.130	0.0813	0.0182	0.0191	0.0162	0.0921	0.0862	0.110
Individual 6	0.0878	0.105	0.0800	0.0330	0.0297	0.0103	0.0789	0.125	0.0971	0.0228	0.0084	0.0259	0.141	0.0607	0.0720

Table 7: Results for Coarse Steps 16 to 20 across dimensions for all individuals

Individual	Coarse Step 21			Coarse Step 22			Coarse Step 23			Coarse Step 24			Coarse Step 25		
	Dim 1	Dim 2	Dim 3	Dim 1	Dim 2	Dim 3	Dim 1	Dim 2	Dim 3	Dim 1	Dim 2	Dim 3	Dim 1	Dim 2	Dim 3
Individual 1	0.0189	0.0173	0.0189	0.0863	0.0856	0.0893	0.122	0.122	0.0847	0.0115	0.0253	0.0244	0.0831	0.117	0.0556
Individual 2	0.0115	0.0245	0.0202	0.130	0.0687	0.0854	0.0226	0.0093	0.0170	0.0803	0.0643	0.129	0.0199	0.0175	0.00972
Individual 3	0.0321	0.0199	0.00940	0.0996	0.0941	0.0779	0.0184	0.0166	0.0226	0.0848	0.0571	0.135	0.00906	0.0245	0.00895
Individual 4	0.0818	0.120	0.0906	0.0204	0.0107	0.0124	0.0826	0.125	0.120	0.108	0.107	0.0973	0.0239	0.0158	0.0167
Individual 5	0.0192	0.0150	0.0133	0.100	0.0790	0.109	0.0205	0.0137	0.0228	0.0992	0.111	0.101	0.0181	0.0174	0.0133
Individual 6	0.0302	0.0235	0.00789	0.0974	0.0732	0.104	0.0298	0.0125	0.00930	0.0819	0.0979	0.0869	0.0188	0.0191	0.0181

Table 8: RMSE averaged across time scale  $l = 1$  for  $t_2 = 21, \dots, 25$  across dimensions for all individuals

Individual	Coarse Step 26			Coarse Step 27			Coarse Step 28			Coarse Step 29			Coarse Step 30		
	Dim 1	Dim 2	Dim 3	Dim 1	Dim 2	Dim 3	Dim 1	Dim 2	Dim 3	Dim 1	Dim 2	Dim 3	Dim 1	Dim 2	Dim 3
Individual 1	0.0126	0.0167	0.0183	0.121	0.0905	0.0828	0.0243	0.0207	0.0220	0.0948	0.105	0.123	0.117	0.1018	0.0918
Individual 2	0.0750	0.1117	0.0931	0.0110	0.0270	0.0198	0.0997	0.121	0.0902	0.0237	0.0207	0.0139	0.0968	0.0806	0.0802
Individual 3	0.104	0.0793	0.100	0.0154	0.0272	0.0280	0.1149	0.0892	0.0803	0.0166	0.0176	0.0207	0.0879	0.0957	0.101
Individual 4	0.107	0.0914	0.0880	0.0231	0.0147	0.0129	0.1120	0.0757	0.0916	0.0151	0.0159	0.0228	0.1098	0.0993	0.101
Individual 5	0.0819	0.0846	0.101	0.0198	0.0136	0.0179	0.0879	0.0957	0.101	0.0303	0.0309	0.0265	0.1070	0.1025	0.0802
Individual 6	0.1069	0.0925	0.0955	0.0128	0.0182	0.0243	0.0870	0.0892	0.131	0.0153	0.0241	0.0175	0.0975	0.0945	0.0788

Table 9: RMSE averaged across time scale  $l = 1$  for  $t_2 = 26, \dots, 30$  across dimensions for all individuals

Individual	Coarse Step 30			Coarse Step 31			Coarse Step 32			Coarse Step 33			Coarse Step 34		
	Dim 1	Dim 2	Dim 3	Dim 1	Dim 2	Dim 3	Dim 1	Dim 2	Dim 3	Dim 1	Dim 2	Dim 3	Dim 1	Dim 2	Dim 3
Individual 1	0.019	0.020	0.011	0.118	0.087	0.105	0.012	0.017	0.013	0.106	0.107	0.087	0.027	0.025	0.026
Individual 2	0.134	0.073	0.106	0.018	0.015	0.021	0.099	0.111	0.087	0.019	0.020	0.021	0.083	0.108	0.126
Individual 3	0.121	0.108	0.067	0.011	0.013	0.014	0.076	0.122	0.089	0.018	0.008	0.018	0.079	0.106	0.149
Individual 4	0.073	0.052	0.073	0.102	0.130	0.112	0.009	0.018	0.017	0.124	0.086	0.112	0.016	0.028	0.020
Individual 5	0.122	0.084	0.103	0.012	0.019	0.016	0.089	0.110	0.084	0.022	0.020	0.027	0.090	0.133	0.080
Individual 6	0.108	0.084	0.095	0.017	0.015	0.013	0.118	0.119	0.091	0.017	0.021	0.012	0.089	0.125	0.093

Table 10: RMSE averaged across time scale  $l = 1$  for  $t_2 = 30, \dots, 34$  across dimensions for all individuals

Individual	Coarse Step 35			Coarse Step 36			Coarse Step 37			Coarse Step 38			Coarse Step 39		
	Dim 1	Dim 2	Dim 3	Dim 1	Dim 2	Dim 3	Dim 1	Dim 2	Dim 3	Dim 1	Dim 2	Dim 3	Dim 1	Dim 2	Dim 3
Individual 1	0.119	0.094	0.101	0.022	0.014	0.016	0.129	0.095	0.093	0.026	0.020	0.016	0.105	0.093	0.115
Individual 2	0.013	0.015	0.023	0.088	0.101	0.115	0.021	0.023	0.028	0.158	0.091	0.087	0.024	0.026	0.025
Individual 3	0.018	0.010	0.013	0.071	0.100	0.105	0.011	0.012	0.013	0.072	0.108	0.123	0.023	0.031	0.025
Individual 4	0.128	0.075	0.097	0.019	0.011	0.028	0.088	0.114	0.105	0.019	0.021	0.016	0.110	0.099	0.122
Individual 5	0.034	0.012	0.020	0.106	0.093	0.122	0.028	0.023	0.011	0.100	0.110	0.129	0.027	0.022	0.011
Individual 6	0.012	0.016	0.015	0.102	0.086	0.077	0.022	0.013	0.031	0.118	0.093	0.096	0.018	0.020	0.033

Table 11: RMSE averaged across time scale  $l = 1$  for  $t_2 = 35, \dots, 39$  across dimensions for all individuals

Individual	Coarse Step 40			Coarse Step 41			Coarse Step 42			Coarse Step 43			Coarse Step 44		
	Dim 1	Dim 2	Dim 3	Dim 1	Dim 2	Dim 3	Dim 1	Dim 2	Dim 3	Dim 1	Dim 2	Dim 3	Dim 1	Dim 2	Dim 3
Individual 1	0.034	0.024	0.012	0.128	0.071	0.098	0.011	0.022	0.013	0.108	0.103	0.121	0.011	0.026	0.014
Individual 2	0.106	0.084	0.102	0.016	0.033	0.030	0.092	0.129	0.104	0.015	0.032	0.020	0.090	0.098	0.089
Individual 3	0.077	0.084	0.126	0.018	0.014	0.024	0.105	0.115	0.087	0.018	0.019	0.028	0.103	0.102	0.107
Individual 4	0.020	0.030	0.030	0.106	0.107	0.085	0.011	0.012	0.015	0.088	0.079	0.095	0.020	0.028	0.021
Individual 5	0.108	0.129	0.076	0.133	0.098	0.073	0.021	0.017	0.028	0.092	0.094	0.104	0.088	0.099	0.137
Individual 6	0.120	0.099	0.113	0.019	0.018	0.024	0.122	0.101	0.089	0.019	0.030	0.024	0.112	0.094	0.085

Table 12: RMSE averaged across time scale  $l = 1$  for  $t_2 = 40, \dots, 44$  across dimensions for all individuals

Individual	Coarse Step 45			Coarse Step 46			Coarse Step 47			Coarse Step 48			Coarse Step 49		
	Dim 1	Dim 2	Dim 3	Dim 1	Dim 2	Dim 3	Dim 1	Dim 2	Dim 3	Dim 1	Dim 2	Dim 3	Dim 1	Dim 2	Dim 3
Individual 1	0.105	0.114	0.084	0.022	0.021	0.027	0.087	0.116	0.086	0.016	0.008	0.023	0.092	0.093	0.120
Individual 2	0.013	0.037	0.033	0.098	0.090	0.121	0.110	0.095	0.109	0.013	0.016	0.015	0.082	0.113	0.095
Individual 3	0.031	0.022	0.032	0.150	0.093	0.067	0.120	0.128	0.070	0.015	0.026	0.010	0.120	0.092	0.093
Individual 4	0.090	0.113	0.093	0.015	0.022	0.011	0.110	0.084	0.104	0.023	0.029	0.011	0.087	0.118	0.085
Individual 5	0.028	0.024	0.029	0.094	0.117	0.086	0.014	0.011	0.010	0.095	0.110	0.116	0.019	0.022	0.022
Individual 6	0.027	0.024	0.011	0.118	0.083	0.095	0.023	0.021	0.030	0.091	0.108	0.116	0.014	0.013	0.021

Table 13: RMSE averaged across time scale  $l = 1$  for  $t_2 = 45, \dots, 49$  across dimensions for all individuals

Individual	Coarse Step 50			Coarse Step 51			Coarse Step 52			Coarse Step 53		
	Dim 1	Dim 2	Dim 3	Dim 1	Dim 2	Dim 3	Dim 1	Dim 2	Dim 3	Dim 1	Dim 2	Dim 3
Individual 1	0.006	0.122	0.103	0.115	0.017	0.029	0.024	0.104	0.124	0.086	0.017	0.008
Individual 2	0.011	0.093	0.140	0.090	0.016	0.019	0.008	0.098	0.080	0.064	0.016	0.030
Individual 3	0.026	0.080	0.096	0.116	0.009	0.014	0.012	0.107	0.097	0.119	0.021	0.025
Individual 4	0.018	0.121	0.072	0.093	0.020	0.014	0.026	0.074	0.153	0.073	0.014	0.015
Individual 5	0.078	0.012	0.027	0.095	0.094	0.069	0.021	0.021	0.030	0.098	0.104	0.074
Individual 6	0.092	0.014	0.010	0.033	0.116	0.086	0.087	0.029	0.024	0.019	0.089	0.117

Table 14: RMSE averaged across time scale  $l = 1$  for  $t_2 = 50, \dots, 53$  across dimensions for all individuals

Individual	Coarse Step 54			Coarse Step 55			Coarse Step 56			Coarse Step 57			Coarse Step 58		
	Dim 1	Dim 2	Dim 3	Dim 1	Dim 2	Dim 3	Dim 1	Dim 2	Dim 3	Dim 1	Dim 2	Dim 3	Dim 1	Dim 2	Dim 3
Individual 1	0.017	0.008	0.019	0.083	0.095	0.110	0.027	0.010	0.027	0.095	0.112	0.120	0.027	0.012	0.021
Individual 2	0.016	0.030	0.035	0.125	0.091	0.051	0.026	0.012	0.016	0.077	0.086	0.122	0.020	0.028	0.020
Individual 3	0.021	0.025	0.029	0.077	0.086	0.085	0.017	0.030	0.027	0.091	0.108	0.075	0.019	0.022	0.020
Individual 4	0.014	0.015	0.026	0.080	0.107	0.111	0.018	0.015	0.012	0.127	0.099	0.099	0.017	0.011	0.023
Individual 5	0.098	0.104	0.074	0.008	0.018	0.024	0.104	0.126	0.102	0.024	0.031	0.017	0.068	0.088	0.126
Individual 6	0.089	0.117	0.118	0.025	0.016	0.009	0.072	0.104	0.107	0.020	0.006	0.020	0.110	0.095	0.093

Table 15: RMSE averaged across time scale  $l = 1$  for  $t_2 = 54, \dots, 58$  across dimensions for all individuals

Individual	Coarse Step 59			Coarse Step 60			Coarse Step 61			Coarse Step 62			Coarse Step 63		
	Dim 1	Dim 2	Dim 3	Dim 1	Dim 2	Dim 3	Dim 1	Dim 2	Dim 3	Dim 1	Dim 2	Dim 3	Dim 1	Dim 2	Dim 3
Individual 1	0.125	0.075	0.080	0.008	0.019	0.028	0.071	0.110	0.124	0.019	0.021	0.022	0.080	0.112	0.125
Individual 2	0.097	0.078	0.127	0.032	0.020	0.027	0.112	0.075	0.097	0.026	0.016	0.020	0.119	0.086	0.084
Individual 3	0.092	0.080	0.120	0.015	0.010	0.015	0.112	0.076	0.124	0.020	0.013	0.009	0.164	0.069	0.095
Individual 4	0.092	0.120	0.100	0.025	0.017	0.021	0.095	0.094	0.096	0.024	0.011	0.028	0.093	0.083	0.081
Individual 5	0.024	0.022	0.017	0.100	0.101	0.083	0.033	0.024	0.029	0.107	0.091	0.097	0.016	0.016	0.015
Individual 6	0.020	0.035	0.026	0.091	0.095	0.079	0.101	0.130	0.103	0.021	0.010	0.022	0.077	0.118	0.102

Table 16: RMSE averaged across time scale  $l = 1$  for  $t_2 = 59, \dots, 63$  across dimensions for all individuals

Individual	Coarse Step 64			Coarse Step 65			Coarse Step 66			Coarse Step 67			Coarse Step 68		
	Dim 1	Dim 2	Dim 3	Dim 1	Dim 2	Dim 3	Dim 1	Dim 2	Dim 3	Dim 1	Dim 2	Dim 3	Dim 1	Dim 2	Dim 3
Individual 1	0.025	0.013	0.028	0.098	0.079	0.104	0.013	0.022	0.020	0.106	0.111	0.075	0.020	0.010	0.028
Individual 2	0.022	0.030	0.022	0.097	0.113	0.070	0.024	0.020	0.012	0.088	0.089	0.137	0.031	0.016	0.019
Individual 3	0.019	0.022	0.026	0.106	0.061	0.070	0.009	0.027	0.014	0.139	0.099	0.061	0.085	0.092	0.132
Individual 4	0.018	0.027	0.017	0.084	0.131	0.091	0.023	0.008	0.013	0.103	0.102	0.112	0.010	0.010	0.020
Individual 5	0.098	0.070	0.102	0.026	0.015	0.023	0.109	0.105	0.093	0.032	0.031	0.032	0.101	0.097	0.096
Individual 6	0.017	0.011	0.010	0.125	0.107	0.078	0.017	0.011	0.032	0.090	0.090	0.106	0.018	0.020	0.023

Table 17: RMSE averaged across time scale  $l = 1$  for  $t_2 = 64, \dots, 68$  across dimensions for all individuals

Individual	Coarse Step 69			Coarse Step 70			Coarse Step 71			Coarse Step 72			Coarse Step 73		
	Dim 1	Dim 2	Dim 3	Dim 1	Dim 2	Dim 3	Dim 1	Dim 2	Dim 3	Dim 1	Dim 2	Dim 3	Dim 1	Dim 2	Dim 3
Individual 1	0.111	0.112	0.112	0.122	0.106	0.094	0.021	0.016	0.018	0.079	0.081	0.071	0.025	0.011	0.018
Individual 2	0.118	0.085	0.095	0.031	0.016	0.019	0.090	0.076	0.082	0.010	0.035	0.028	0.101	0.098	0.092
Individual 3	0.008	0.022	0.025	0.076	0.124	0.094	0.022	0.017	0.019	0.113	0.096	0.107	0.020	0.021	0.016
Individual 4	0.103	0.105	0.090	0.025	0.021	0.025	0.084	0.115	0.082	0.029	0.027	0.025	0.068	0.124	0.115
Individual 5	0.023	0.019	0.036	0.069	0.133	0.080	0.023	0.023	0.016	0.093	0.084	0.102	0.023	0.024	0.013
Individual 6	0.080	0.085	0.095	0.027	0.022	0.026	0.105	0.101	0.083	0.011	0.006	0.022	0.113	0.102	0.107

Table 18: RMSE averaged across time scale  $l = 1$  for  $t_2 = 69, \dots, 73$  across dimensions for all individuals

Individual	Coarse Step 74			Coarse Step 75			Coarse Step 76			Coarse Step 77			Coarse Step 78		
	Dim 1	Dim 2	Dim 3	Dim 1	Dim 2	Dim 3	Dim 1	Dim 2	Dim 3	Dim 1	Dim 2	Dim 3	Dim 1	Dim 2	Dim 3
Individual 1	0.119	0.093	0.085	0.018	0.024	0.010	0.101	0.101	0.082	0.012	0.014	0.022	0.103	0.114	0.099
Individual 2	0.024	0.009	0.019	0.106	0.082	0.095	0.024	0.026	0.021	0.091	0.102	0.112	0.020	0.024	0.015
Individual 3	0.089	0.087	0.086	0.097	0.111	0.108	0.036	0.021	0.008	0.101	0.109	0.084	0.015	0.015	0.021
Individual 4	0.023	0.018	0.031	0.095	0.118	0.083	0.017	0.012	0.019	0.114	0.102	0.103	0.010	0.018	0.013
Individual 5	0.105	0.087	0.097	0.016	0.016	0.014	0.102	0.126	0.096	0.020	0.011	0.023	0.095	0.108	0.081
Individual 6	0.023	0.013	0.017	0.097	0.103	0.106	0.033	0.030	0.016	0.106	0.093	0.112	0.021	0.007	0.020

Table 19: RMSE averaged across time scale  $l = 1$  for  $t_2 = 74, \dots, 78$  across dimensions for all individuals

Individual	Coarse Step 79			Coarse Step 80			Coarse Step 81			Coarse Step 82			Coarse Step 83		
	Dim 1	Dim 2	Dim 3	Dim 1	Dim 2	Dim 3	Dim 1	Dim 2	Dim 3	Dim 1	Dim 2	Dim 3	Dim 1	Dim 2	Dim 3
Individual 1	0.009	0.012	0.015	0.099	0.098	0.113	0.015	0.022	0.020	0.107	0.111	0.076	0.033	0.024	0.017
Individual 2	0.100	0.132	0.081	0.013	0.011	0.025	0.124	0.127	0.078	0.022	0.010	0.015	0.099	0.075	0.117
Individual 3	0.078	0.104	0.095	0.017	0.020	0.016	0.096	0.083	0.114	0.023	0.024	0.014	0.079	0.111	0.113
Individual 4	0.125	0.113	0.082	0.090	0.115	0.129	0.032	0.023	0.016	0.102	0.102	0.105	0.028	0.017	0.006
Individual 5	0.019	0.013	0.027	0.103	0.120	0.100	0.018	0.027	0.014	0.104	0.097	0.101	0.019	0.023	0.021
Individual 6	0.108	0.087	0.097	0.016	0.012	0.029	0.098	0.129	0.075	0.024	0.009	0.020	0.063	0.065	0.072

Table 20: RMSE averaged across time scale  $l = 1$  for  $t_2 = 79, \dots, 83$  across dimensions for all individuals

Individual	Coarse Step 84			Coarse Step 85			Coarse Step 86			Coarse Step 87			Coarse Step 88		
	Dim 1	Dim 2	Dim 3	Dim 1	Dim 2	Dim 3	Dim 1	Dim 2	Dim 3	Dim 1	Dim 2	Dim 3	Dim 1	Dim 2	Dim 3
Individual 1	0.106	0.102	0.085	0.024	0.021	0.014	0.098	0.124	0.096	0.018	0.018	0.019	0.101	0.122	0.075
Individual 2	0.012	0.010	0.016	0.094	0.087	0.099	0.026	0.026	0.020	0.082	0.118	0.115	0.022	0.019	0.023
Individual 3	0.019	0.023	0.016	0.130	0.105	0.075	0.011	0.018	0.015	0.095	0.099	0.110	0.024	0.030	0.018
Individual 4	0.115	0.090	0.110	0.123	0.103	0.106	0.019	0.024	0.016	0.115	0.087	0.098	0.020	0.015	0.015
Individual 5	0.093	0.131	0.096	0.012	0.020	0.021	0.117	0.086	0.095	0.128	0.108	0.080	0.009	0.018	0.013
Individual 6	0.017	0.021	0.017	0.090	0.122	0.104	0.018	0.020	0.020	0.101	0.096	0.082	0.007	0.016	0.015

Table 21: RMSE averaged across time scale  $l = 1$  for  $t_2 = 84, \dots, 88$  across dimensions for all individuals

Individual	Coarse Step 89			Coarse Step 90			Coarse Step 91			Coarse Step 92			Coarse Step 93		
	Dim 1	Dim 2	Dim 3	Dim 1	Dim 2	Dim 3	Dim 1	Dim 2	Dim 3	Dim 1	Dim 2	Dim 3	Dim 1	Dim 2	Dim 3
Individual 1	0.026	0.013	0.017	0.063	0.129	0.085	0.016	0.017	0.010	0.114	0.122	0.084	0.150	0.091	0.097
Individual 2	0.080	0.089	0.093	0.020	0.025	0.023	0.085	0.102	0.097	0.016	0.014	0.008	0.097	0.106	0.106
Individual 3	0.093	0.067	0.131	0.007	0.023	0.010	0.056	0.074	0.096	0.024	0.009	0.022	0.104	0.074	0.108
Individual 4	0.084	0.091	0.076	0.022	0.014	0.020	0.079	0.101	0.114	0.012	0.023	0.019	0.123	0.114	0.089
Individual 5	0.090	0.135	0.093	0.140	0.097	0.092	0.024	0.016	0.017	0.110	0.090	0.091	0.028	0.021	0.014
Individual 6	0.109	0.107	0.107	0.100	0.123	0.060	0.024	0.023	0.009	0.099	0.090	0.126	0.013	0.014	0.033

Table 22: RMSE averaged across time scale  $l = 1$  for  $t_2 = 89, \dots, 93$  across dimensions for all individuals

Individual	Coarse Step 94			Coarse Step 95			Coarse Step 96			Coarse Step 97		
	Dim 1	Dim 2	Dim 3	Dim 1	Dim 2	Dim 3	Dim 1	Dim 2	Dim 3	Dim 1	Dim 2	Dim 3
Individual 1	0.025	0.014	0.017	0.084	0.101	0.115	0.021	0.018	0.014	0.092	0.084	0.083
Individual 2	0.018	0.028	0.019	0.091	0.092	0.118	0.025	0.019	0.016	0.103	0.107	0.097
Individual 3	0.018	0.016	0.017	0.080	0.099	0.100	0.020	0.025	0.017	0.060	0.092	0.079
Individual 4	0.016	0.010	0.014	0.101	0.114	0.097	0.016	0.030	0.024	0.119	0.071	0.094
Individual 5	0.105	0.113	0.084	0.023	0.013	0.013	0.116	0.101	0.096	0.026	0.026	0.027
Individual 6	0.112	0.087	0.096	0.102	0.141	0.099	0.009	0.021	0.010	0.089	0.105	0.109

Table 23: RMSE averaged across time scale  $l = 1$  for  $t_2 = 94, \dots, 97$  across dimensions for all individuals

Individual	Coarse Step 98			Coarse Step 99			Coarse Step 100		
	Dim 1	Dim 2	Dim 3	Dim 1	Dim 2	Dim 3	Dim 1	Dim 2	Dim 3
Individual 1	0.022	0.022	0.038	0.081	0.098	0.121	0.014	0.024	0.024
Individual 2	0.014	0.031	0.021	0.112	0.102	0.095	0.010	0.021	0.008
Individual 3	0.017	0.016	0.029	0.094	0.082	0.112	0.016	0.021	0.029
Individual 4	0.020	0.019	0.013	0.116	0.077	0.094	0.011	0.013	0.015
Individual 5	0.102	0.138	0.076	0.019	0.028	0.020	0.081	0.124	0.107
Individual 6	0.023	0.020	0.014	0.143	0.092	0.079	0.009	0.009	0.022

Table 24: RMSE averaged across time scale  $l = 1$  for  $t_2 = 98, \dots, 100$  across dimensions for all individuals